

We would like to thank the referees for their time and useful comments to help improve this manuscript. Hereby our replies to the different points which were addressed by referee #2. The *referee comments* are given in italic blue, our replies in black. The page and line numbers mentioned refer to the non-revised AMTD manuscript. A revised version of the manuscript highlighting the changes made (with latexdiff) is attached at the end.

In the course of the review, we stumbled on an error in one of the calculations in the validation scripts. This error had an impact on the validation results. Therefore chapter 5 has been adjusted. The figures and table have been updated as well as the text. We sincerely apologize for this. The changes made are listed at the end after addressing the different referee comments.

## GENERAL COMMENTS

My main concern is that, having read the paper in some detail, I am still unsure of the quality of the measurements, regarding both the influence of the a priori and the error analysis.

We will hereby address these point in order to give clarity to the referee on the quality of our product by outlining a more detailed error analysis and by showing that the atmospheric CH<sub>4</sub> variations observed are a result of the variability of atmospheric CH<sub>4</sub> rather than the a priori information.

1) The authors state that the CH<sub>4</sub> a priori comes from a WACCM climatology but does this a single global/time average, is it zonal/seasonal, or something else? Assuming it has some latitude/seasonal dependence then the question arises: to what extent are the latitude/seasonal cycles depicted in the maps and NDACC comparisons simply reproducing the a priori variations rather than the CH<sub>4</sub> retrieval? One way of testing this would be to subtract the a priori from both the data and the NDACC sites and examine the statistics with which \*variations\* from the climatology are reproduced.

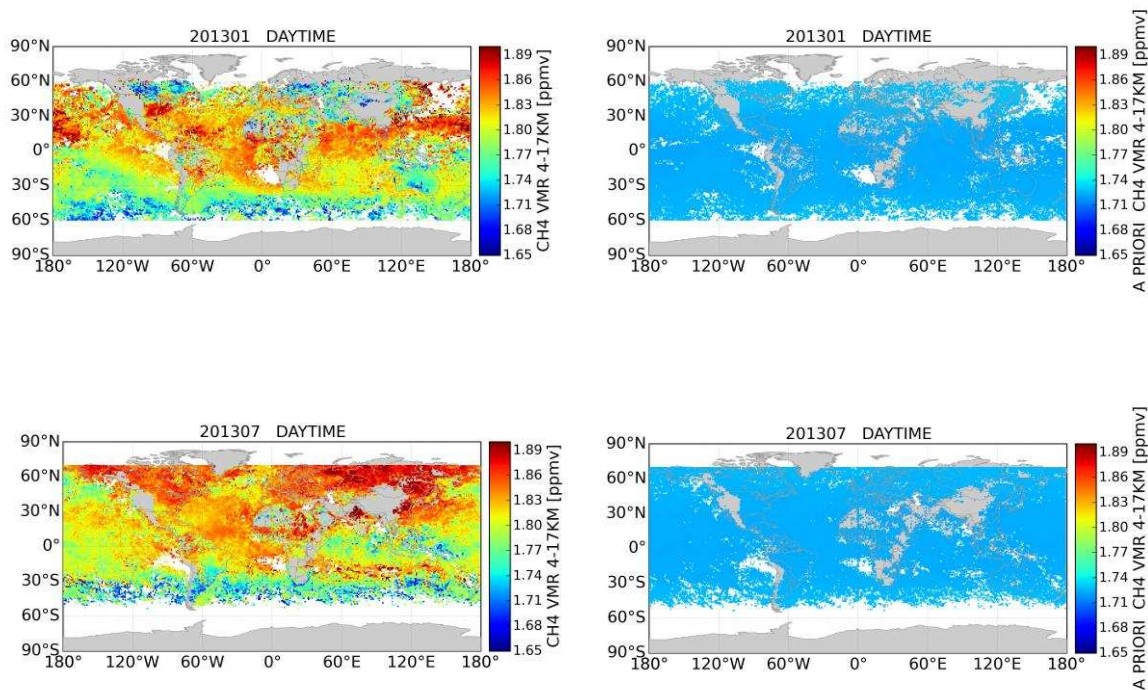
This would be a more accurate measure of the added value of the IASI measurements compared to just assuming climatology. Another test, assuming the climatology has no trend, would be to compare time series with the annual cycles removed, but that would probably require more than 3 years of data. While there are plots showing the a priori (smoothing) error contribution to the individual profile levels, there is nothing equivalent for the a priori contribution to the 3-17km partial column which is presented for NDACC comparisons.

This was indeed not clearly mentioned in the manuscript.

The a priori profile is a single CH<sub>4</sub> profile used for all latitudes and seasons. It therefore shows no latitudinal/seasonal dependence. The choice for a single a priori profile is, as the referee mentions, to **not** introduce any variability in the final retrieved product from the a priori variability. Below we show 4 figures. On the left hand side 2 figures of retrieved IASI CH<sub>4</sub> for January 2013 and July 2013 (as in Fig. 8) and on the right hand side the CH<sub>4</sub> a priori is given, which is constant at all latitudes and for the different seasons. As you can see, we use one single CH<sub>4</sub> a priori profile.

In Sect. 3.2 we added the following text to make sure there is no unclarity regarding the a priori profile used :

A single global CH<sub>4</sub> xa profile is used for all the retrievals, representative of a mid-latitude CH<sub>4</sub> profile. Therefore the atmospheric CH<sub>4</sub> variations observed are a results of the variability of atmospheric CH<sub>4</sub> rather than the a priori information.



Review-Figure 1 : [left] Monthly mean global daytime distribution of CH<sub>4</sub> partial columns (4-17 km) in 2013, as given in Figure 8 of the manuscript. [right] A priori CH<sub>4</sub> partial columns (4-17 km) for the same 2 months.

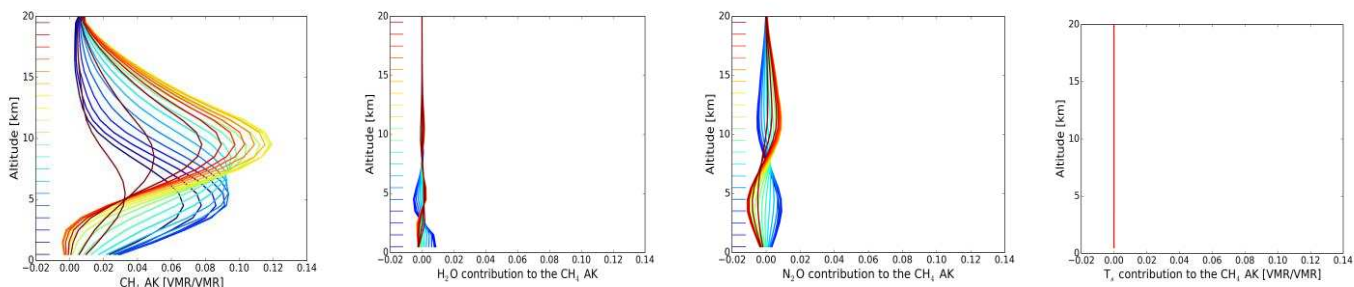
2) For the 'reference' paper for any new satellite dataset I feel there should really be a quantitative 'bottom up' error analysis, ie an formal assessment of the magnitudes of the various error terms based on internal tests, which can then be compared by the authors (or other users), to independent data for a 'top down' approach. That is really lacking in this paper. The errors would presumably include contributions from all of the following: instrument noise, errors in retrieved temperature, surface emissivity errors, residual cloud contamination, a priori biases, concentrations of interfering molecules (including HDO) PCC reconstruction error, spectroscopic errors - see specific comments below. These all seem to be handled in the retrieval as a diagonal covariance matrix of fixed size approx 5x noise, and in the NDACC comparisons not assessed at all. An assessment of random error, or precision, could simply be obtained from the SD of the 2x2 pixels or some other small area where it is assumed the CH<sub>4</sub> concentration is relatively uniform. It would be useful to have some figures for all these terms, even if only upper limits, for the 3-17km partial column which seems to be the basic product.

We added a section Error Analysis in which we calculate the error budget of the IASI CH<sub>4</sub> 4-17 km partial column.

Here we include the values of the smoothing and measurement uncertainties as estimated following the formalism by Rodgers (2000) and as was discussed in Section 3.2. Additionally we estimate the uncertainty on the CH<sub>4</sub> 4-17km partial column by additional error sources such as the temperature profile, the emissivity and spectroscopic parameters by a perturbation method. This analysis gives an

estimate of the random and systematic uncertainty of the IASI CH<sub>4</sub> 4-17km partial column product.

The parameters considered in the state vector; the interfering species H<sub>2</sub>O and N<sub>2</sub>O, and the skin temperature have no significant contribution to the uncertainty of the CH<sub>4</sub> product. This can be seen from the contribution of these species to the CH<sub>4</sub> averaging kernel. In the figure below the CH<sub>4</sub> averaging kernel (AK) is given (left), and the contribution of the other parameters in the state vector on the CH<sub>4</sub> AK, the H<sub>2</sub>O profile (2nd figure), the N<sub>2</sub>O profile (3rd figure) and the skin temperature T<sub>s</sub> (figure on the right).



Review-Figure 2: [left] IASI CH<sub>4</sub> averaging kernel (AK), as is given in Figure 2 of the manuscript. The contribution of the additional parameters in the state vector to the CH<sub>4</sub> AK; H<sub>2</sub>O [2<sup>nd</sup> figure from the left], N<sub>2</sub>O [3<sup>rd</sup> figure from the left], and the skin temperature (T<sub>s</sub>) [right].

Nevertheless, we considered the uncertainty of the spectroscopic parameters of the 2 dominant interfering species N<sub>2</sub>O and H<sub>2</sub>O + isotopes and found an insignificant contribution to the CH<sub>4</sub> retrieved values. The PCC uncertainty is estimated by comparing the difference in retrieved CH<sub>4</sub> from the PCC radiances and the raw radiances.

The following section (Section 4.3) discussing the error sources and their contribution was added to the manuscript:

In Sect. 3.2 we discussed the two error sources which contribute to the total retrieval error: the smoothing error, which accounts for the low vertical resolution of the retrievals, and the measurement error. Their uncertainties are estimated following Rodgers (2000) and are shown in Fig. 2. Additional sources of error propagating into the total retrieval error are due to uncertainties in forward model parameters or ancillary data used in the inversions. These error sources are currently not explicitly taken into account in the ASIMUT retrieval software. We therefore estimated the uncertainties by forward model parameters or ancillary data by a perturbation method, following Barret et al. (2002, 2003). A set of spectra in a latitude-longitude band between 60°S-70°N and 120-125°E were selected, comprising a set of 4000 spectra. This is a representative set for the latitudinal coverage of the IASI CH<sub>4</sub> dataset, with spectra over land and water. For the different error sources considered, IASI CH<sub>4</sub> is retrieved for this set of spectra with the original set-up and the uncertainty added to the specific error source. The uncertainty of this error source on the IASI CH<sub>4</sub> partial column is then estimated as the difference between the newly retrieved IASI CH<sub>4</sub> partial column (with the uncertainty of the error source added) and the IASI CH<sub>4</sub> partial column from the current optimized retrieval set-up. The

different error sources and their uncertainties are listed in Table 2, as well as the results of the estimated uncertainties of the IASI CH<sub>4</sub> 4-17 km partial column for each individual error source.

The uncertainty of the temperature profile on the CH<sub>4</sub> partial column is estimated by substituting the IASI L2 temperature profiles with the ECMWF ERA-Interim (Dee et al., 2011) re-analysis temperature profiles. ECMWF ERA-Interim re-analysis data is available at 6 hourly intervals with a horizontal resolution of  $\sim 0.75^\circ$  in latitude and longitude. The temperature profiles are interpolated to the location and time of the IASI pixel and the retrieved CH<sub>4</sub> is compared with the CH<sub>4</sub> partial column of the optimized retrieval set-up. For the CH<sub>4</sub> absorption lines the uncertainty on the line intensity, the air and self broadening coefficients is set to 2%. This is consistent with what García et al. (2017) considered in their uncertainty estimation. For the interfering species, N<sub>2</sub>O, H<sub>2</sub>O and isotopologues, which are simultaneously retrieved, we also set the uncertainties on the spectroscopic parameters (line intensity and air and self broadening coefficients) to 2%. We also estimated a systematic uncertainty of the IASI CH<sub>4</sub> a priori of 2%. Following García et al. (2017) the uncertainty on the emissivity is 1% for all wavenumbers. For the PCC uncertainty we calculated the difference between IASI CH<sub>4</sub> retrieved from PCC spectra and from raw spectra, as already shown in Sect. 3.3. The smoothing and measurement uncertainty are estimated as in Sect. 3.2.

The third column in Table 2 lists the results. The dominant sources of error are the smoothing error and the CH<sub>4</sub> line intensity with an uncertainty on the IASI CH<sub>4</sub> 4-17 km partial column of 2.45% and 1.93% respectively. Other error sources contributing significantly to the uncertainty of the CH<sub>4</sub> 4-17 km partial column are the temperature profile (1.40%), the CH<sub>4</sub> broadening coefficients (1.09%) and the measurement uncertainty (0.95%). There is also a non-negligible contribution of the emissivity uncertainty of 0.27%. Uncertainties in the spectroscopic parameter of N<sub>2</sub>O, H<sub>2</sub>O and its isotopologues do not significantly contribute to the uncertainty in CH<sub>4</sub>. The systematic uncertainty of the IASI CH<sub>4</sub> a priori also has a negligible effect of 0.06%. Combining the different contributions to the IASI CH<sub>4</sub> error budget, we estimated a total uncertainty on the CH<sub>4</sub> 4-17 km partial column of 3.73%. If we consider the temperature, measurement, PCC reconstruction and smoothing uncertainty as random error sources we get an estimate of the precision of the IASI CH<sub>4</sub> 4-17 km partial column of 2.98%. If we consider uncertainties in the spectroscopy and emissivity as systematic error sources, the systematic uncertainty of the CH<sub>4</sub> 4-17 km partial column is 2.23%.

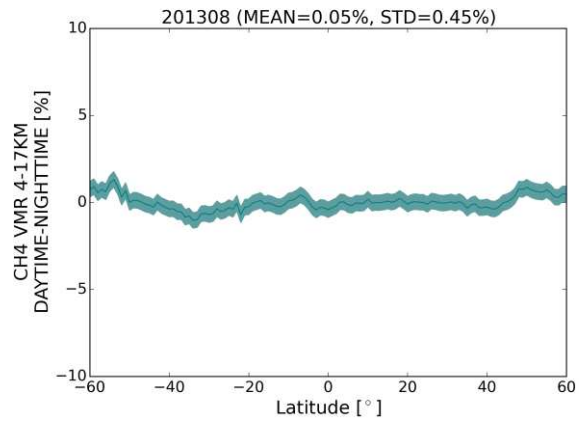
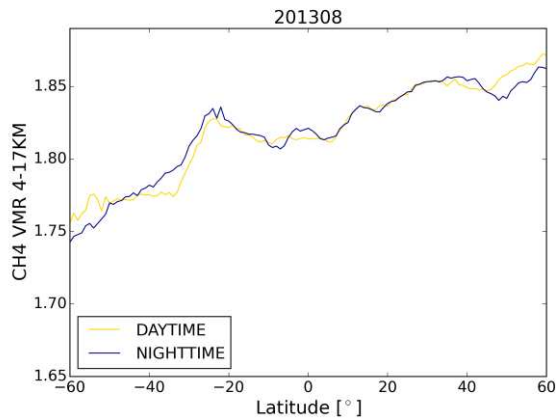
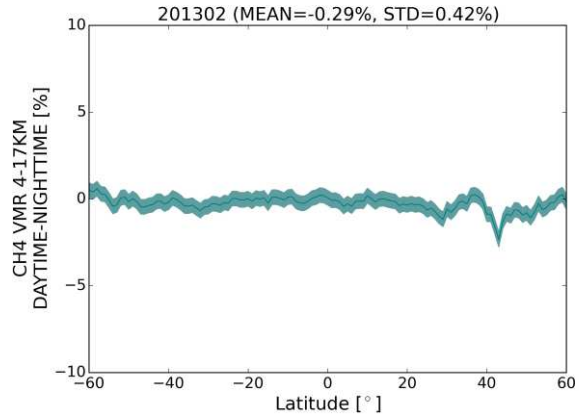
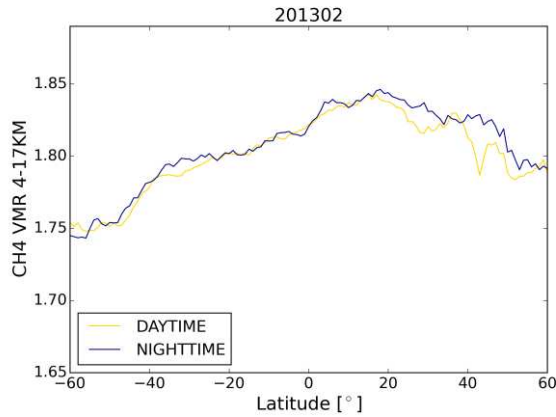
Error Source	Uncertainty Error Source	Uncertainty IASI CH <sub>4</sub>
Temperature profile	-	1.40%
CH <sub>4</sub> line intensity	2%	1.93%
CH <sub>4</sub> broadening coefficients	2%	1.09%
CH <sub>4</sub> a priori bias	2%	0.06%
H <sub>2</sub> O line intensity	2%	0.02%
H <sub>2</sub> O broadening coefficients	2%	0.03%
N <sub>2</sub> O line intensity	2%	0.05%
N <sub>2</sub> O broadening coefficients	2%	0.03%
PCC reconstructed	-	0.02%
Emissivity	1%	0.27%
Smoothing	a priori variability	2.45%
Measurement noise	$2 \cdot 10^{-8} \text{W}/(\text{cm}^2 \text{sr cm}^{-1})$	0.95%
Total		3.73%

**Table 2.** The different error sources (column 1) and their uncertainties considered (column 2) for the IASI CH<sub>4</sub> uncertainty estimation. The results of the uncertainty estimation of the CH<sub>4</sub> 4-17 km partial columns by the perturbation method described in Sect. 4.3 are given in column 3. The uncertainty of the temperature profile on the CH<sub>4</sub> 4-17 km partial column is estimated by replacing the IASI L2 temperature profiles with the ECMWF Era-interim re-analysis temperature profiles. To estimate the uncertainty of the PCC reconstructed spectra on the CH<sub>4</sub> columns we used the raw spectra and compared the retrieved CH<sub>4</sub> partial columns with the PCC reconstructed retrieved CH<sub>4</sub> as is done in Sect. 3.3.

*And a couple more suggestions, which I leave to the authors' to include or not:*

3) Since both day and night are processed separately, although one would not expect the CH<sub>4</sub> to change significantly over a diurnal cycle, I would also like to know if the day and night zonal means are self-consistent within the error budgets.

Indeed, one does not expect for CH<sub>4</sub> to change significantly over a diurnal cycle. The differences between day and nighttime retrieved CH<sub>4</sub> would mostly be due to differences in sensitivity due to different thermal contrast conditions. In the figure below (Figure 3) the daytime and nighttime zonal means are given for 2 months, February and August 2013, as well as their relative differences. The mean relative difference between daytime and nighttime zonal means is -0.29% and 0.05% for February and August 2013 respectively. These values are well below the uncertainties estimated from the error analysis of Section 4.3 (2.63% considering only the smoothing and measurement uncertainty and 3.73% considering the additional error sources as temperature profile, emissivity and spectroscopy). We decided not to include this in the manuscript, but hope the referee finds these results satisfactory.



Review-Figure 3: [left] Zonal mean CH<sub>4</sub> 4-17 km partial columns in vmr for February and August 2013 for daytime (yellow) and nighttime (purple) measurements. [right] Relative differences of daytime and nighttime zonal mean measurements (solid line) with the 1-sigma standard deviation given by the colored area. The mean difference and standard deviation of the difference are given in the title.

4) A simpler error analysis could be to use the WACCM profiles to convert both NDACC and IASI to total CH<sub>4</sub> column amounts.

Thank you for the suggestion but we decided that the error analysis based on the perturbation method outlined in Section 4.3 is a more detailed and thorough estimate of the CH<sub>4</sub> error budget.

## SPECIFIC COMMENTS

*P1,L1: The product is described as 'global' but results are only shown for 60S-70N.*

Indeed. The term 'global' has been removed.

A new global IASI methane product developed at ..

→

A new IASI methane product developed at ..

*P1,L4: 'retrieval uncertainty ... less than 4%'. Be a bit more specific about whether this refers to precision (ie random error), or accuracy (total error, including systematic biases) - ideally quote both.*

With the Error Analysis added (Section 4.3) we changed this to:

The retrieval uncertainty of the CH<sub>4</sub> profiles is less than 4% below 100 hPa (~16 km).

→

An detailed error analysis was performed. The total uncertainty is estimated to be 3.73% for a CH<sub>4</sub> partial column between 4-17 km.

*P1,L10: 'absolute differences ... less than 1%'. Again, not clear what this means, 'Absolute' usually means irrespective of +/- sign, and difference could be anything from single-profile match ups to mean bias throughout the whole dataset.*

We changed this and also added the term 'Relative mean differences'. Changes were also made with respect to the revised validation results.

P1, L9:

Mean differences between IASI and FTIR CH<sub>4</sub> range between -1.93 and 4.40% and are within the systematic uncertainty.

For 7 out of the 10 stations absolute differences are less than 1%.

→

Relative mean differences between IASI and FTIR CH<sub>4</sub> range between -2.31 and 4.04% and are within the systematic uncertainty. For 6 out of the 10 stations the relative mean differences are smaller than ±1%.

*P2,L29: The other IASI CH<sub>4</sub> products, currently cited only in the Conclusion, should also be mentioned here at the start to put this work into its proper context.*

This has been added :

..METOP-B in September 2012 (Razavi et al., 2009; Crevoisier et al., 2009; Xiong et al., 2013).

→

..METOP-B in September 2012 (Razavi et al., 2009; Crevoisier et al., 2009; Xiong et al., 2013; Siddans et al., 2016; Garcia et al., 2017).

*P3,L4: The final section also contains a significant description of proposed future work.*

Indeed, thank you, we added this.

The final section summarizes the main results of this work.

→

The final section summarizes the main results of this work and discusses future work.

*P3,L6: Pedantically, since there is mention of MetOp-B and MetOp-C, there should be some mention of MetOp-A. And presumably it's not just IASI that will provide a 15 year dataset but all, or at least most, of the other MetOp payload instruments as well.*

We changed MetOp to MetOp-A.

The Infrared Atmospheric Sounding Interferometer (IASI) onboard MetOp is a thermal..

→

The Infrared Atmospheric Sounding Interferometer (IASI) onboard MetOp-A is a thermal..

*P3,L14: 'four spectral bands' - I thought there were only three? (breaks at 1210 and 2000cm-1). Also, emphasise that these actually provide a continuous spectrum, without gaps (unlike several other FTIR instruments).*

Indeed, thank you for pointing that out. We changed the following:

IASI has four spectral bands in the spectral range from 645 to 2760 cm-1 ..

→

IASI has three spectral bands in the spectral range from 645 to 2760 cm-1 (3.62 to 15.5 μm), provided as a continuous spectrum with an apodized spectral resolution of 0.5 cm-1 and spectral sampling of 0.25 cm-1.

*P4,L2: No reference given for Drummond et al.*

Thank you. We added the reference of Drummond et al.:

Drummond, R., Vandaele, A.-C., Daerden, F., Fussen, D., Mahieux, A., Neary, L., Neefs, E., Robert, S., Willame, Y., and Wilquet, V.: Studying methane and other trace species in the Mars atmosphere using a SOIR instrument, *Planetary and Space Science*, 59, 292–298, <http://www.sciencedirect.com/science/article/pii/S0032063310001479>, 2011

*P4,L8: The EUMETSAT L2 skin temperature is also used as an input (P4,L23).*

We changed this.

EUMETSAT IASI L2 temperature and water vapour profiles are used as input for the radiative transfer calculations.

→

EUMETSAT IASI L2 skin temperature (T<sub>skin</sub>), temperature and water vapour profiles are used as input for the radiative transfer calculations.

*P4,L11: Is this the dataset commonly referred to as the 'Wicsonsin' surface emissivity data? And what is used over the ocean?*

I'm not familiar how this dataset is commonly referred to, but I don't think it's the same one. The Zhou emissivity/climatology database generated from IASI measurements (0.5°x0.5°) we received from Dan Zhou includes emissivity values over land and over water.

*P4,L15: What molecule do these 'problem' features belong to? Are they the CH4 Q-branches? And does the forward model include CH4 line-mixing? Also, have the effects of the variation in HDO been considered?*

We have not been able to identify that yet. It could be a combination of line mixing or uncertainties in the HDO spectroscopy.

Our forward model does not include CH<sub>4</sub> line mixing. Razavi. et al. (2009) investigated the impact of line mixing in the nu<sub>4</sub> spectral band of CH<sub>4</sub>. They showed that the most influential impact was around the methane Q branch around 1306 cm-1 and they therefore excluded the Q branch from the retrieval window. We followed their reasoning.

These features are not part of the Q branch, this spectral region is the CH<sub>4</sub> nu<sub>4</sub> P branch.

The isotopologues of the different molecules included are considered in our forward model, so we do include HDO.

P4,L16: Setting the radiometric noise to infinity (or very large) is the mathematical way to exclude spectral points from the retrieval, not setting the noise to zero. And if these points are excluded from *the fit, in what sense is 'no information lost'?*

Sorry, indeed, we mean the signal to noise is set to 0, thank you for pointing this out. This has been corrected. If you would take several spectral windows, to exclude these spectral points, instead of the whole spectral region we are taking now (1210-1290 cm<sup>-1</sup>), your information content will be reduced. By masking these spectral points we don't lose information content.

We changed the following:

These spectral ranges are masked in the retrieval set-up, i.e. the radiometric noise is set to zero at these spectral points..

→

These spectral ranges are masked in the retrieval set-up, i.e. the signal-to-noise is set to zero at these spectral points..

P4,L18: Is there any evidence that the 10% cloud fraction does not contribute a significant error? One might hope that the skin temperature, or other non-CH<sub>4</sub> elements of the state vector, will absorb any residual cloud, but that also depends on the tightness of the a priori constraints. I expect the EUMETSAT skin temperature is retrieved with a very small error, so may not allow for much cloud-compensation within the CH<sub>4</sub> retrieval. A plot of bias and SD v CH<sub>4</sub> a priori, or zonal mean, or NDACC, as a function of cloud percentage would answer this.

What we actually see is that taking a fractional cloud cover < 10% based on the EUMETSAT IASI L2 fractional cloud fraction corresponds to a 0% fractional cloud coverage. We therefore can't generate a figure of the retrieved CH<sub>4</sub> as a function of cloud percentage.

We'd like to point out that many other trace gas retrieval products of IASI use a less constrained filtering of cloud contaminated spectra. F.e. for the IASI NH<sub>3</sub> (Van Damme et al. 2014) and HNO<sub>3</sub> (Ronsmans et al., 2016) products spectra with a fractional cloud cover <25 % are processed.

P4,L22: Is the 23-level state vector an arbitrary choice or is it set by the EUMETSAT L2 or WACCM profiles used as a priori data?

The 23-level state vector is an arbitrary choice.

P4,L28: Is there a reason for imposing a uniform a priori uncertainty for H<sub>2</sub>O rather than using the uncertainty associated with the EUMETSAT H<sub>2</sub>O product that is actually used for the a priori profile? Even if just for scaling the diagonal elements.

The EUMETSAT H<sub>2</sub>O product has an accuracy of 10% which we set here as the standard deviation of the IASI L2 H<sub>2</sub>O a priori. Initial tests with different H<sub>2</sub>O uncertainties/covariance matrices, gave us the most optimal retrieval results for a uniform covariance matrix with a 10% standard deviation and correlation length of 6 km.

P4,L24: I assume this means that the climatology is some sort of average of the WACCM model output - global, annual mean? monthly zonal mean? - while the covariance represents the model statistical variability about this mean. *If the WACCM output is on the same levels as your retrieval grid that's quite straightforward, but if it isn't then there are a few more steps involved.*

A single global CH<sub>4</sub> x<sub>a</sub> profile is used for all the retrievals, representative of a mid-latitude CH<sub>4</sub> profile. The other referee also asked for additional information, so we added the following text in the manuscript on P4, L24:

The a priori profiles x<sub>a</sub> and covariance matrices S<sub>a</sub> for CH<sub>4</sub> and N<sub>2</sub>O are based on a climatology from the WACCM model. A single CH<sub>4</sub> a priori profile, representative for a mid-latitude CH<sub>4</sub> profile, is used for all latitudes and seasons. Therefore the atmospheric CH<sub>4</sub> variations observed are a result of

the variability of atmospheric CH<sub>4</sub> rather than the a priori information. The CH<sub>4</sub> covariance matrix represents the highest variability at the surface and in the upper troposphere-lower stratosphere (UTLS). The variability in the UTLS is representative for the variability of the CH<sub>4</sub> gradient at the tropopause which is different at different latitudes.

P4, L29: The characterisation of forward model errors as a simple scaling of the nominal noise diagonal matrix is certainly convenient but requires a little more justification than just the plain statement presented here. The fact that PCC reconstructed radiances agree within the nominal radiometric noise (Fig 3) for a single spectrum is not in itself sufficient to demonstrate that the reconstruction error is negligible: unlike the radiometric noise the reconstruction error is likely to have significant and persistent correlations with the spectrum itself, so unlike the random noise, the impact will generally not be reduced as  $1/\sqrt{n}$ , where  $n$  is the number of spectral points used.

As discussed in general comment #2, a section with a more detailed error analysis of the IASI CH<sub>4</sub> 4-17 km partial column has now been added (Section 4.3).

Indeed, the reconstruction process is likely to introduce spectral correlations. However, comparing the retrieved partial columns of CH<sub>4</sub> of PCC spectra with raw radiances in the perturbation theory and as shown in Section 3.3 (Figure 4), we found this error source negligible in comparison to other error sources such as spectroscopy, the temperature profile, emissivity..

P5,L1: The shape of the averaging kernels presumably depends significantly on the surface *temperature contrast*, but that information is not given with the figure. It's hardly surprising that, with DOFS~1, the profile uncertainty is dominated by the a priori error, or 'smoothing error'. A more useful figure would be the error in a quantity which more realistically represents the retrieval information, eg integrated total or partial column amount, and how this compares with the a priori uncertainty. It certainly makes for a more meaningful comparison with other CH<sub>4</sub> retrievals which are on different profile levels.

The uncertainties are now added for the 4-17 km partial columns in Section 4.3. The uncertainty values of the different error sources are listed in Table 2 to give a more meaningful comparison with other CH<sub>4</sub> retrieval products.

P5,L2: Here the effective sampling range is defined as 2-16 km but elsewhere 4-17 km columns are used.

The wording of this sentence make it seem like a generalized statement for the whole IASI CH<sub>4</sub> dataset indeed. We changed the sentence as follows:

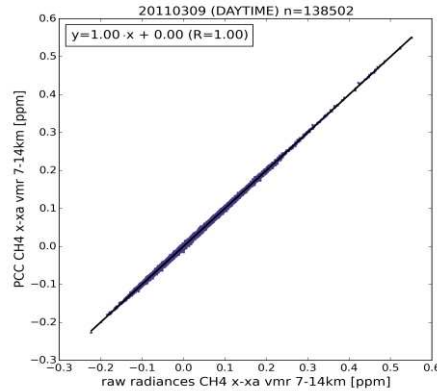
It shows that the sensitivity of the IASI CH<sub>4</sub> product lies in the 800-100 hPa (~2-16 km) range.

→

It shows that the sensitivity of the retrieved IASI CH<sub>4</sub> profile lies in the 800-100 hPa (~2-16 km) range.

P5,L20: The correlation plot Fig 4 is used as evidence that the PCC reconstruction error is negligible. However, this is a comparison of absolute CH<sub>4</sub> values which, as already demonstrated in Fig 2, are closely constrained by the a priori, so a good correlation may only represent the fact that the measurements have little influence on the a priori. I would be more convinced by a plot of the correlation of the \*differences\* with respect to the a priori profile.

We're not 100% sure we understand the referee correctly here. Under the assumption we use a variable a priori CH<sub>4</sub> profile (over location and time), indeed the correlation may represent the variability in the a priori if we're not sensitivity to the measurement. However this is not the case, we use 1 single a priori profile. Looking at the correlation of the difference wrt the a priori would then just be subtracting a constant. We added this figure here for the referee just to be clear, for 1 day in March 2011 :



P5,L31: From Google maps I conclude that these 3 locations are all over the sea – but it would be *helpful to state that in the text or the figure caption. If you have only three examples, I don't think it is useful to present both northern and southern mid-latitudes, which one would expect to be similar (particularly near the equinox). It would be more informative to have different land-air temperature contrasts instead, representing the max/min values shown in Fig 6.*

Indeed, they all seem to be over the sea. We have created these figures randomly and want to give the reader a quick overview on the shape of the averaging kernel, at different geographical locations. Of course, these are 'just 3 examples' but they are representative of the general conditions we get at mid-latitudes and in the tropics. We believe they are more informative than giving the averaging kernels at the max/min thermal contrast values. Figure 7 gives a more elaborate overview of the whole range of sensitivity of the IASI CH4 measurements.

We regenerated a few figures and replaced the 2 figures on the left to have not just 3 locations over the sea. The averaging kernels are very much the same.

We changed the caption of Figure 5 accordingly:

CH4 averaging kernels for 3 pixels on the 1st of March 2013 at 3 different locations (55°N, 4°N and 47°S)

→

CH4 averaging kernels for 3 pixels on the 1st of March 2013 at 3 different locations (52°N, 4°N and 47°S)

In the text we changed :

P5,L31:

..at 3 different geographical locations; at northern mid-latitudes (55°N), in the tropics..

→

..at 3 different geographical locations; at northern mid-latitudes (52°N), in the tropics..

P6,L4:

One independent piece of information (1.01 < DOFS < 1.47)..

→

One independent piece of information (1.01 < DOFS < 1.45)..

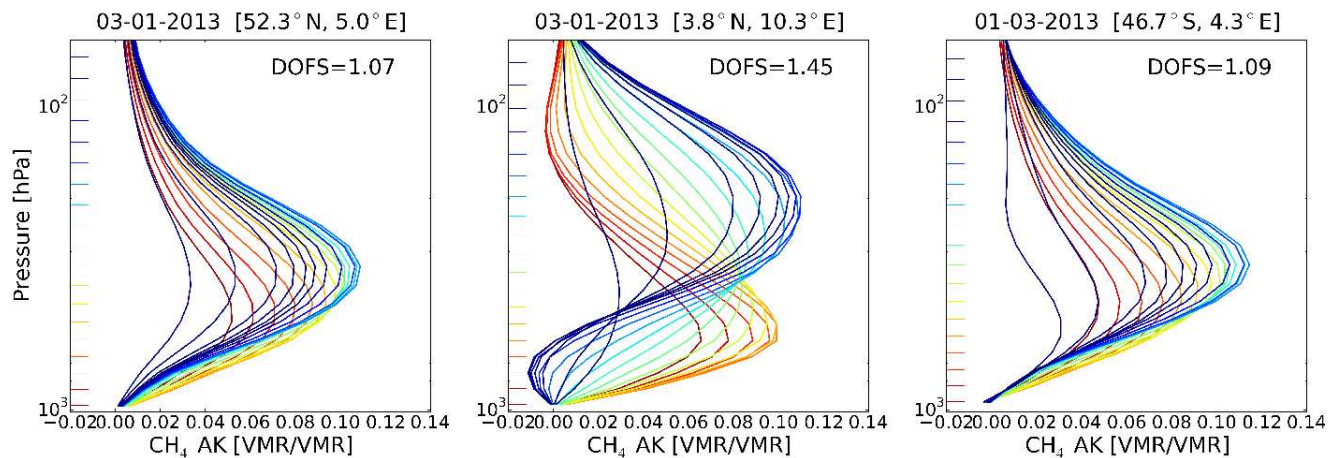


**Figure 5.** CH<sub>4</sub> averaging kernels for 3 pixels on the 1<sup>st</sup> of March 2013 at 3 different locations (52°N, 4°N and 47°S).

*P6,L10: 'thermal contrast' needs to be defined.*

We changed the sentence (P6, L10):

The variability of the AK (and hence the DOFS) is dependent on the thermal contrast..

→

The variability of the AK and hence the DOFS is dependent on the thermal contrast (the difference between the surface temperature and the temperature of the first atmospheric vertical layer)..

*P6,L20: 'one independent piece of information is retrieved with good sensitivity'. While DOFS ~ 1, it would be more useful to have some idea of, for example, how this translates to a reduction in the a priori uncertainty for a 4-17km column.*

Section 4.1 on Information content explains the vertical sensitivity of the retrieved profile. We believe it's important that the reader of the manuscript understands that although a profile of CH<sub>4</sub> is retrieved there is only one piece of information, which is what we would like to stress in this chapter. We therefore like to keep this section as it is, with the information as is given.

*P6,L23: What limits the latitude coverage? Here it says 60S-70N but two of the NDACC comparison sites are higher than 70N.*

P6, L23: The limits were chosen to produce the necessary dataset for the GHG-CCI project. For the NDACC validation the CH<sub>4</sub> profiles were retrieved at the different NDACC station locations and consequently at two NDACC sites at latitudes higher than 70°N.

*P6,L23: 'binned on a 1x1 deg grid'. So does this mean the plotted points represent not just an average of the four pixels but an average of all the pixels within the 1x1 box? Or is the binning some other process? And what happens if, say one of the 4 pixels is flagged as cloud-contaminated. Is the average then made of the remaining 3 or is this set of 4 pixels excluded?*

It is the average of all the pixels within the 1x1 degree box. If one of the 4 pixels is flagged as cloud-contaminated the set of 4 pixels is excluded.

*P8,L24 gives IASI a priori systematic component as 2% of a priori value. Where does this come from? Just the error in WACCM? No systematic component of IASI retrieval uncertainty is considered.*

P8, L24: The 2% a priori systematic component is an estimate that the a priori values at certain locations could be under- or overestimated. We assume 1 single a priori profile for the whole globe whose values could easily be underestimated at certain locations.

References: not in alphabetical order, some missing publication year, and inconsistently formatted. Patra 2009 listed in references but not cited in text.

We double checked all the references and added the bibliography now with a bibtex file.

Fig 1: Rather than just show a generic piece of spectrum it would be helpful if this figure was also used to show the individual contributions of different molecules to this spectral region (eg separate panel with same x-axis).

We added a separate panel with the contributions of the different molecules, see the figure below.

We changed the caption of figure 2 accordingly:

[top] Measured (blue) and simulated (yellow) radiances. [bottom] Measured minus simulated radiances. The mean difference (bias),  $1-\sigma$  standard deviation of the difference and radiometric noise-value used in the retrieval (all in  $\times 10^{-8} \text{ W}/(\text{cm}^2 \text{ sr cm}^{-1})$ ) are given in the title.

→

Top panel : [top] Measured (blue) and simulated (yellow) radiances. [bottom] Measured minus simulated radiances. The mean difference (bias),  $1-\sigma$  standard deviation of the difference and radiometric noise-value used in the retrieval (all in  $\times 10^{-8} \text{ W}/(\text{cm}^2 \text{ sr cm}^{-1})$ ) are given in the title. Bottom panel : Three simulated radiances under the assumption of a single-species atmosphere containing either only CH<sub>4</sub>, H<sub>2</sub>O or N<sub>2</sub>O, showing the contribution of the different prominent molecules in this spectral region.

And added the following sentences in the text on P4, L12 :

In the lower panel, the overlapping contributions of the different molecules CH<sub>4</sub>, H<sub>2</sub>O and N<sub>2</sub>O are illustrated. Here the radiances are simulated under the assumption of a single-species atmosphere containing either CH<sub>4</sub>, H<sub>2</sub>O or N<sub>2</sub>O. The top panel shows a negligible bias and..

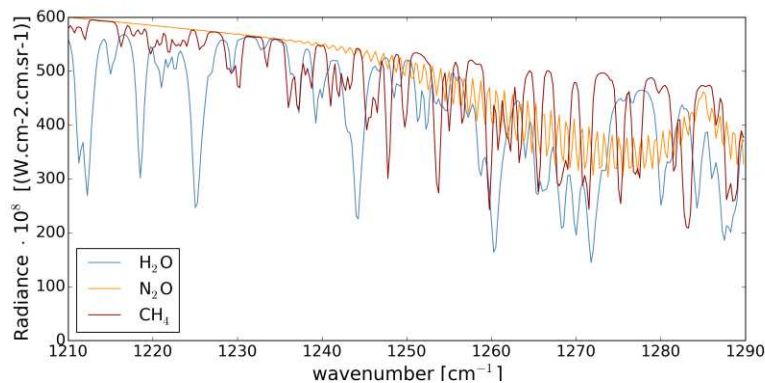
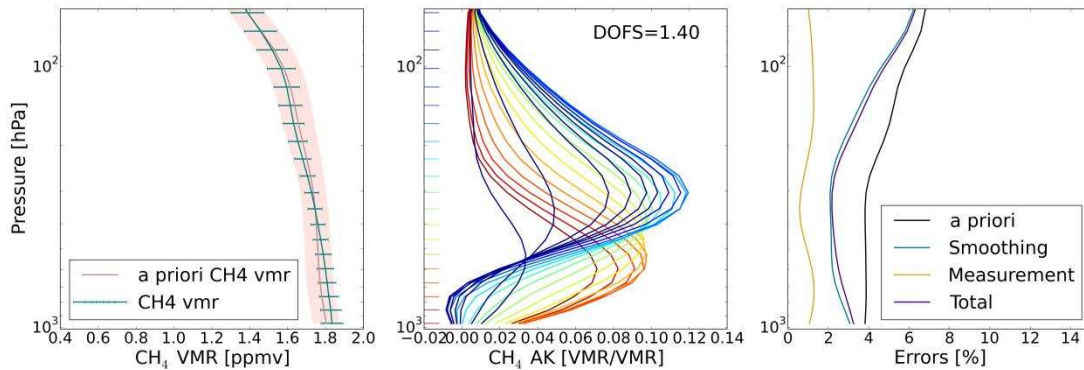


Fig 2: On the left panel it would be helpful to also have the a priori error bars plotted for comparison.

We added a shaded area in Fig. 2 which represents the a priori variability as calculated from the square root of the diagonal of the a priori covariance matrix. We added the following sentence to the caption of Fig.2:

The pink shaded area is the a priori variability and the horizontal blue bars are the retrieval uncertainty.



**Figure 2.** [left] Retrieved and a priori CH<sub>4</sub> vmr profile in ppmv for an observation on the 2<sup>nd</sup> of July 2013. The pink shaded area is the a priori variability and the horizontal blue bars are the retrieval uncertainty. [middle] Averaging kernel of the retrieval with a DOFS of 1.40. [right] CH<sub>4</sub> uncertainty profiles in percentage. Given are the measurement (yellow) and smoothing (blue) uncertainty which contribute to the total (purple) uncertainty. The black line represents the variability of the a priori as calculated from the square root of the diagonal elements of the a priori uncertainty covariance matrix  $S_a$ .

Table 1: This lists a priori information as WACCM, but that is only for certain elements of the state vector. 'IASI L2' should include the word 'EUMETSAT' for consistency with the text. There should also be something about the a priori covariance information.

Table 1: IASI L2 has been added to the a priori information. The description in the text (Sect 3.2) regarding the a priori covariance information is in my opinion sufficient.

Table 2: I'm surprised at the spread in systematic errors in Table 2 for the various NDACC comparisons. Assuming this represents a combination of the NDACC systematic error budget and the 2% systematic error assumed for the retrieval a priori, this variation must mostly come from the NDACC data. Yet Sepulveda et al (2014) quotes a figure of 2.5% which is largely spectroscopic uncertainty (and therefore common to all sites). And the fact that these systematic errors are all much larger than the biases suggests something wrong.

The spread in systematic uncertainties in Table 2 is indeed due to the variation in systematic uncertainty estimates of the NDACC dataset which is not consistent for the different NDACC stations. As mentioned in the text, the NDACC CH<sub>4</sub> retrieval is not fully harmonized yet. The implementation of a fully harmonized retrieval is ongoing work as part of the GAIA-CLIM project. A harmonization of the uncertainty estimates is also part of that work. Sepulveda et al. (2014) did a separate study where they analyzed the spectra at 9 NDACC stations with a different inversion code PROFFIT (the NDACC FTIR community uses the SFIT software) and they did a separate error analysis. This is not the same data that is publicly available on the NDACC data site.

We added the following 2 sentences on P8, L33:

They were found to be less than 1% for 6 out of the 10 NDACC stations. As mentioned before, a full harmonization of the NDACC CH<sub>4</sub> retrieval is ongoing..

→

They were found to be less than 1% for 6 out of the 10 NDACC stations. Also note the spread in uncertainty estimates, especially for the systematic component. This is due to the differences in

reported systematic and random error covariances from the different NDACC stations. As mentioned before, a full harmonization of the NDACC CH<sub>4</sub> retrieval is ongoing..

### TYPOGRAPHICAL ERRORS/SUGGESTIONS

We implemented the corrections the referee suggested. Thank you for being so observant.

P1,L3: usefullness → usefulness

P2,L2: greenhouse gas-intensive → greenhouse gas-intensive

P2,L3 + P2,L7 + P2,L9 + P9,20 + P19, caption Figure 4: ppb → ppbv

P2,L5 + P16,L6 :WMO News Bulletin, 2016 → WMO News Bulletin, 2016).

P2,L31: LIDAR → lidar

P3,L6:

The Infrared Atmospheric Sounding Interferometer (IASI) onboard MetOp, is a thermal cross-nadir scanning infrared sounder.

→ The Infrared Atmospheric Sounding Interferometer (IASI) onboard MetOp is a thermal cross-nadir scanning infrared sounder.

P3,L7:

Launched in October 2006, it is the first in a successive series of three..

→ Launched in October 2006, it is the first in a series of three..

P3,L16:

..for numerical weather predictions, the IASI mission..

→ ..for numerical weather prediction, the IASI mission..

P3,L19: On the longer term the continuity of the program is ensured.. → In the longer term the continuity of the programme is ensured..

P3,L20: ..the IASI observation.. → ..the IASI observations..

P3,L23: ASIMUT-ALVL is a modular software for radiative transfer (RT) calculations.. → ASIMUT-ALVL is modular software for radiative transfer (RT) calculations..

P4,L3: ..instrument on-board ExoMars.. → ..instrument onboard ExoMars..

P4,L8:

The spectral range considered for the CH<sub>4</sub> retrieval is the 1210-1290 cm<sup>-1</sup> range covering part of the v<sub>4</sub> spectral band. →

The spectral range considered for the CH<sub>4</sub> retrieval is the 1210-1290 cm<sup>-1</sup> region covering part of the v<sub>4</sub> spectral band.

P4,L12: ..and its residual.. → ..and the residual..

P4,L14: Certain spectral ranges in the considered spectral band.. → Certain spectral ranges in the considered spectral region..

P4,L22: ..are summarized in Table 6. → ..are summarized in Table 61.

P4,L28: ..its a priori.. → ..their a priori..

P4,L32: water vapor → water vapour

P5,L3: diplays → displays

P4,L5: .. constrained with of an a priori.. → ..constrained with an a priori..

P4,L11: su rface → surface

P5,L17: ..10 Tb which is reduced to 1 Tb/year.. → ..10 Tb which is reduced to 1 Tb..

P5,L19:  $4 \times 10^{-9} \text{ W}/(\text{m}^2 \text{ sr m}^{-1})$  →  $4 \times 10^{-9} \text{ W}/(\text{cm}^2 \text{ sr cm}^{-1})$

P5, L20:  $2 \times 10^{-8} \text{ W}/(\text{m}^2 \text{ sr m}^{-1})$  →  $2 \times 10^{-8} \text{ W}/(\text{cm}^2 \text{ sr cm}^{-1})$

P5,L24: negligibles → negligible

P6,L30: van Weele et al. (2011) examined.. → Van Weele et al. (2011) examined..

P7,L17: ..with less than 200 collocations.. → ..with fewer than 200 collocations..

P8,L5: alitude → altitude

P8,L30: slighlty → slightly

P12,L32: Forc- ing → Forcing

Fig 1: insert space: 'sr cm'  
This has been implemented.

### References

Ronsmans, G., Langerock, B., Wespes, C., Hannigan, J. W., Hase, F., Kerzenmacher, T., Mahieu, E., Schneider, M., Smale, D., Hurtmans, D., De Maziere, M., Clerbaux, C., and Coheur, P.-F.: First characterization and validation of FORLI-HNO<sub>3</sub> vertical profiles retrieved from IASI/Metop, Atmos. Meas. Tech., 9, 4783-4801, <https://doi.org/10.5194/amt-9-4783-2016>, 2016.

Van Damme, M., Clarisse, L., Heald, C. L., Hurtmans, D., Ngadi, Y., Clerbaux, C., Dolman, A. J., Erisman, J. W., and Coheur, P. F.: Global distributions, time series and error characterization of atmospheric ammonia (NH<sub>3</sub>) from IASI satellite observations, Atmos. Chem. Phys., 14, 2905-2922, <https://doi.org/10.5194/acp-14-2905-2014>, 2014.

## **CHANGES VALIDATION RESULTS:**

### **ABSTRACT**

IASI CH<sub>4</sub> partial columns are found to correlate well with the ground-based data for 7 out of the 10 Fourier Transform Infrared (FTIR) stations with correlation coefficients between 0.71 and 0.96. Mean differences between IASI and FTIR CH<sub>4</sub> range between -1.93 and 4.40% and are within the systematic uncertainty. For 7 out of the 10 stations absolute differences are less than 1%. The standard deviation of the difference lies between 1.40 and 3.99% for all the stations.

→

IASI CH<sub>4</sub> partial columns are found to correlate well with the ground-based data for 6 out of the 10 Fourier Transform Infrared (FTIR) stations with correlation coefficients between 0.60 and 0.84. Relative mean differences between IASI and FTIR CH<sub>4</sub> range between -2.31 and 4.04% and are within the systematic uncertainty. For 6 out of the 10 stations the relative mean differences are smaller than ±1%. The standard deviation of the difference lies between 1.76 to 2.97% for all the stations.

### **SECT. 5 VALIDATION**

P8, L5:

.. where the FTIR measurement has maximum sensitivity (typically at 5km altitude on the LOS).

→

.. where the FTIR measurement has maximum sensitivity (typically at 5km altitude on the LOS). To guarantee a certain homogeneity of the NDACC data with NDACC CH<sub>4</sub> profiles of comparable quality we applied a filtering on some of the NDACC data when large outliers were found. We also applied a filtering to the IASI CH<sub>4</sub> profiles. We omitted IASI pixels with DOFS < 0.85 and when the root mean square of the residual >  $2.2 \times 10^{-8}$  W/(cm<sup>2</sup> sr cm<sup>-1</sup>).

P8, L9:

Relative mean differences between IASI and NDACC lie between -1.93 and 0.67% (of which 7 stations out of 10 less than ±1%) with exception of the Thule station, where IASI is biased high with respect to NDACC by 4.4%. The standard deviation of the difference lies in the range 1.91 to 3.99% for the 10 stations.

→

Relative mean differences between IASI and NDACC lie between -2.31 and 0.18% (of which 6 stations out of 10 less than ±1%) with exception of the Thule station, where IASI is biased high with respect to NDACC by 4.04%. The standard deviation of the difference lies in the range 1.76 to 2.97% for the 10 stations.

P8, L29:

Also for Thule the mean difference of 4.40% is within the systematic uncertainty of 5.14%.

→

Also for Thule the mean difference of 4.04% is within the systematic uncertainty of 5.28%.

P8, L30:

The standard deviation of the difference is close to the random uncertainty, but for certain stations slightly larger. This discrepancy could be due to an additional error associated with the grid conversions or a geolocation error which are not taken into account (Calisesi et al., 2005; Vigouroux et al., 2009). Another reason could be the current underestimation of the random uncertainty of the NDACC CH<sub>4</sub> retrievals. They were found to be less than 1% for 6 out of the 10 NDACC stations. The ongoing work in the GAIA-CLIM project will harmonize the error characterization for all NDACC stations in the coming period. This comparison stresses the importance of this harmonization work.

→

The standard deviation of the difference is within the random uncertainty for all stations. We did notice a current underestimation of the random uncertainty of the NDACC CH<sub>4</sub> retrievals. They were found to be less than 1% for 6 out of the 10 NDACC stations. Also note the spread in uncertainty estimates, especially for the systematic component. This is due to the differences in reported systematic and random error covariances from the different NDACC stations. The ongoing work in the GAIA-CLIM project will harmonize the error characterization for all NDACC stations in the coming period. This comparison stresses the importance of this harmonization work.

P9, L2:

Scatter plots of collocated partial columns are presented in Fig. 10. We find very good correlations ( $R=0.71-0.88$ ) for the high-latitude stations Eureka, Thule and Kiruna. High correlations ( $R>0.9$ ) are found as well for the mid-latitude stations Jungfraujoch and Zugspitze, while the mid-latitude station Toronto performs poorer with a correlation of 0.44. The tropical island stations Maito and Mauna Loa show poor correlations ( $R=0.41-0.50$ ) although biases are below 1% for these stations. The tropical island station Izaña however shows a high correlation of 0.90. For the most Southern station Wollongong (34°S) we find a good correlation of 0.77. The poorer correlations at the Mauna Loa, Maito and Toronto stations could be attributed to the lower CH<sub>4</sub> variability we see at these locations compared to the other stations. In addition, at Mauna Loa and Toronto, we see a few outliers which could explain the poorer linear regression fit at these stations. These results demonstrate the ability of the IASI data to well capture the temporal variation of CH<sub>4</sub>.

→

Scatter plots of collocated partial columns are presented in Fig. 10. We find good correlations ( $R=0.67-0.84$ ) for the high-latitude stations Eureka, Thule and Kiruna. Good correlations are found as well for the mid-latitude stations Jungfraujoch ( $R=0.81$ ) and Zugspitze ( $R=0.68$ ), while the mid-latitude station Toronto performs poorer with a correlation of 0.52. The tropical island stations Izaña, Maito and Mauna Loa show poor correlations ( $R=0.15-0.36$ ) although biases are below 1.20% for these stations. For the most Southern station Wollongong (34°S) we find a correlation of 0.60. Several tests were performed to explain the poorer correlations found at the tropical island stations. We applied a stronger filtering on the IASI and NDACC data but found no improvement. We investigated a possible relation of IASI land or IASI sea pixels with differences between the IASI and NDACC retrieved CH<sub>4</sub> but found no correlation. We therefore attribute the poorer correlations at the Izaña, Mauna Loa and Maito stations to the lower CH<sub>4</sub> variability we see at these locations compared to the other stations. In addition, at Maito and Mauna Loa, we see a few outliers which could explain the poorer linear regression fit at these stations.

## SECT. 6 DISCUSSION, CONCLUSION AND OUTLOOK

P9, L25 :

Mean difference values range between -1.93 and 4.40% for the 10 stations. Absolute differences are less than 1% for 7 stations out of 10. The standard deviation of the difference lies in the range 1.91 to 3.99% for all the stations. These values are close to the random uncertainty of IASI and NDACC, but for certain stations slightly larger. Possible reasons for this discrepancy could be an underestimation of the NDACC CH<sub>4</sub> random uncertainty or additional error sources not considered in the calculation of the random uncertainty, such as a regriding or geolocation error. Very good correlations are found for 7 out of the 10 NDACC stations with correlation coefficients between 0.71 and 0.96. Particularly for the 3 high-latitude stations we find high correlations, as well as for the 2 high-quality mid-latitude stations Jungfraujoch and Zugspitze. With these results we are confident that the IASI data is capturing the mid to upper CH<sub>4</sub> variability well.

->

Mean difference values range between -2.31 and 4.04% for the 10 stations. Absolute differences are less than 1% for 6 stations out of 10. The standard deviation of the difference lies in the range 1.76 to 2.97% for all the stations. These values are within the random uncertainty of IASI and NDACC. Very good correlations are found for 6 out of the 10 NDACC stations with correlation coefficients between 0.60 and 0.84. Particularly for the 3 high-latitude stations we find high correlations, as well as for the 2 high-quality mid-latitude stations Jungfraujoch and Zugspitze.

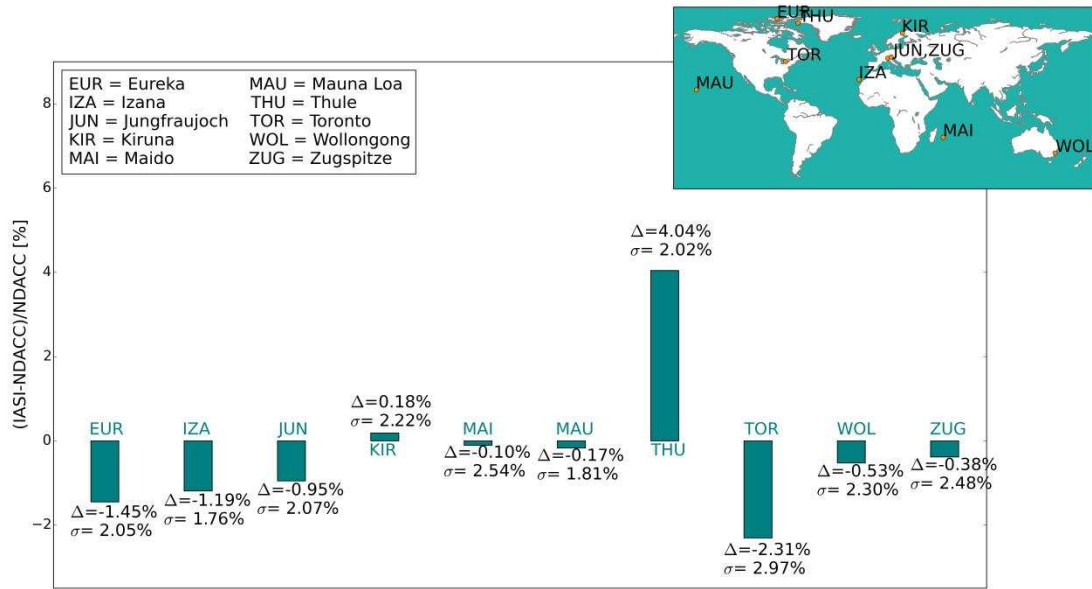


**Figure 9.** Barchart of the results of the IASI-NDACC validation exercise. Given is the relative percentage difference  $\Delta=(IASI-NDACC)/NDACC$  and standard deviation of the difference ( $\sigma$ ) of partial columns in the 4-17 km altitude range for each of the 10 investigated NDACC sites, visualized in the map on the top right. These results are also summarized in Table 3.

site	LAT	$\Delta$ [%]	$\sigma$ [%]	$\epsilon_{sys}$ [%]	$\epsilon_{rand}$ [%]	R	n
Eureka	80°N	-1.45	2.05	7.63	2.65	0.67	373
Thule	77°N	4.04	2.02	5.28	2.58	0.73	209
Kiruna	68°N	0.18	2.22	3.59	2.71	0.84	437
Jungfrauoch	47°N	-0.95	2.07	NA	NA	0.81	674
Zugspitze	47°N	-0.38	2.48	2.21	2.56	0.68	2020
Toronto	44°N	-2.31	2.97	8.26	3.21	0.52	535
Izana	28°N	-1.19	1.76	3.29	2.46	0.37	3290
Mauna Loa	20°N	-0.17	1.81	4.75	2.48	0.33	592
Maida	21°S	-0.10	2.54	3.44	2.89	0.15	478
Wollongong	34°S	-0.53	2.30	6.70	6.21	0.60	2230

**Table 3.** Statistics of the comparison between the IASI and smoothed NDACC CH<sub>4</sub> 4-17 km partial columns for the period 2011-2014. For each location, the latitude coordinates, the mean percentage difference ( $\Delta=(IASI-NDACC)/NDACC$ ) and standard deviation of the difference ( $\sigma$ ), the mean systematic ( $\epsilon_{sys}$ ) and random uncertainty of the differences ( $\epsilon_{rand}$ ), the correlation coefficient (R) and the number of observations (n) are given. NA=not available, for Jungfrauoch the systematic and random uncertainty covariance matrices are not available.

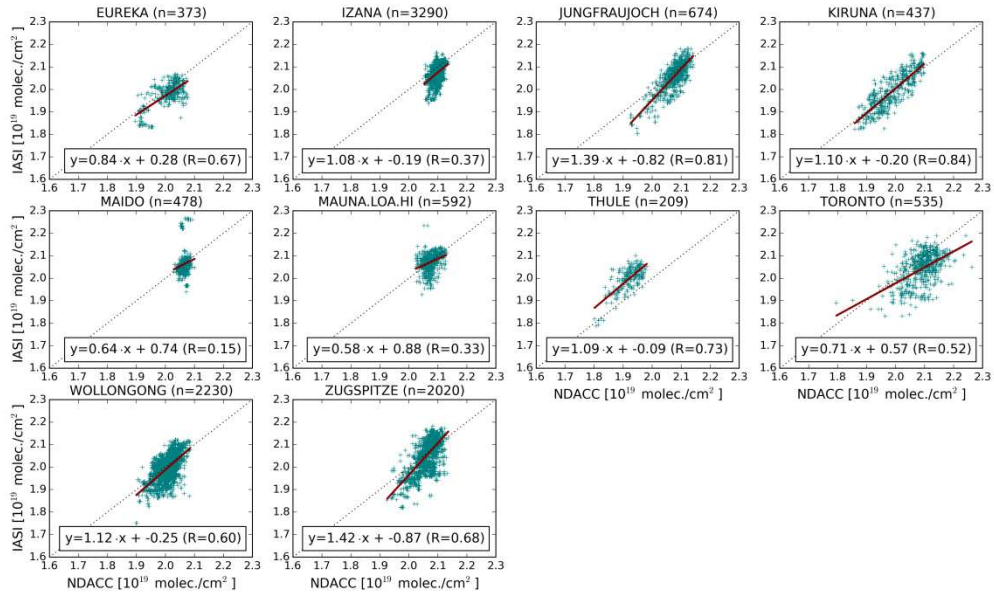


**Figure 10.** Correlation plots of smoothed NDACC and IASI CH<sub>4</sub> partial columns (4-17 km) in molec./cm<sup>2</sup> for the period 2011-2014. The number of collocations (n) is given for each site in the title. The red lines are the linear regressions between the data points and the dashed black line is the unity slope, shown for comparison. The values of the linear regression and the correlation coefficient (R) are given for each station, the latter is summarized in Table 3.



# Retrieval and validation of ~~METOP~~MetOp/IASI methane

Evelyn De Wachter<sup>1</sup>, Nicolas Kumps<sup>1</sup>, Ann Carine Vandaele<sup>1</sup>, Bavo Langerock<sup>1</sup>, and Martine De Mazière<sup>1</sup>

<sup>1</sup>Royal Belgian Institute for Space Aeronomy (BIRA-IASB), 1180 Brussels, Belgium

*Correspondence to:* Evelyn De Wachter (evelyn.dewachter@aeronomie.be)

**Abstract.** A new ~~global~~IASI methane product developed at the Royal Belgian Institute for Space Aeronomy (BIRA-IASB) is presented. The retrievals are performed with the ASIMUT-ALVL software based on the Optimal Estimation Method (OEM). This paper gives an overview of the forward model and retrieval concept. The ~~usefulness~~usefulness of reconstructed Principal Component Compressed (PCC) radiances is highlighted. The ~~retrieval uncertainty of the CH<sub>4</sub> profiles is less than 4% below~~  
5 ~~100 hPa (~16 km).~~The information content study carried out in this paper shows that most IASI pixels contain between 0.9 and 1.6 independent pieces of information about the vertical distribution of CH<sub>4</sub>, with a good sensitivity in the mid to upper troposphere. A detailed error analysis was performed. The total uncertainty is estimated to be 3.73% for a CH<sub>4</sub> partial column between 4-17 km. An extended validation with ground-based CH<sub>4</sub> observations at 10 locations was carried out. IASI CH<sub>4</sub> partial columns are found to correlate well with the ground-based data for ~~7~~6 out of the 10 Fourier Transform Infrared (FTIR)  
10 stations with correlation coefficients between ~~0.71 and 0.96.~~Mean ~~0.60 and 0.84.~~Relative mean differences between IASI and FTIR CH<sub>4</sub> range between ~~-1.93 and 4.40~~-2.31 and 4.04% and are within the systematic uncertainty. For ~~7~~6 out of the 10 stations ~~absolute differences are less than~~the relative mean differences are smaller than ±1%. The standard deviation of the difference lies between ~~1.40 and 3.99~~1.76 to 2.97% for all the stations.

## 1 Introduction

15 There is now a widespread scientific consensus on the profound influence of human activity on the global climatic system, particularly through increased emissions of greenhouse gases like ~~carbon dioxide (CO<sub>2</sub> and)~~and methane (CH<sub>4</sub>) since the pre-industrial era (Jardine et al., 2009). Although CH<sub>4</sub> is roughly 200 times less abundant in the atmosphere than CO<sub>2</sub>, it is a more potent greenhouse gas. The comparative impact of CH<sub>4</sub> on climate change is more than 86 times greater than CO<sub>2</sub> over a 20-year period (~~?~~(Myhre et al., 2013)). Identified CH<sub>4</sub> emission sources are either of biogenic, pyrogenic or thermo-  
20 genic origin. CH<sub>4</sub> emissions of biogenic origin are related to anaerobic decomposition; a collection of processes by which microorganisms break down organic matter in the absence of oxygen. Examples are natural wetlands, oxygen-poor freshwater reservoirs, digestive systems of ruminants, rice paddies and waste treatment (Kirschke et al., 2013). Pyrogenic CH<sub>4</sub> is produced by the incomplete combustion of biomass and soil carbon during wildfires and of biofuels and fossil fuels. Thermogenic sources comprise the exploitation of oil, natural gas and coal and the natural degassing from the subsurface such as terrestrial  
25 seeps, marine seeps and mud volcanoes (Kirschke et al., 2013). The primary sink for atmospheric CH<sub>4</sub> is oxidation by hydroxyl radicals (OH), mostly in the troposphere, which accounts for about 90% of the global CH<sub>4</sub> sink (Kirschke et al., 2013).

In addition, CH<sub>4</sub> is depleted at the surface by consumption by soil bacteria and by its reaction with chlorine radicals in the marine boundary layer. These processes amount to a lifetime of atmospheric CH<sub>4</sub> of ~9 years.

Since 2014, atmospheric CH<sub>4</sub> concentrations are rising faster than at any time in the past two decades and ~~are its concentration~~ is now approaching the most greenhouse ~~gas-intensive scenarios (Saunois et al., 2016)~~ gas intensive Representative Concentration

5 Pathway (RCP) trajectories (Saunois et al., 2016), the scenario pathways which were introduced by the Intergovernmental Panel on Climate Change (IPCC) in its fifth Assessment Report (AR5) in 2014. Its concentration has more than doubled since the pre-industrial period, reaching a new high of  $1845 \pm 2$  ~~ppb~~ ppbv in 2015, an increase of 11 ~~ppb~~ ppbv with respect to the previous year, as shown by the latest analysis of observations from the World Meteorological Organization (WMO) Global Atmosphere Watch (GAW) Programme (WMO, 2016). CH<sub>4</sub> is a challenging atmospheric component to study as its non-  
10 monotonous changes in the last decades and its interannual variability remain not fully understood (Nisbet et al., 2014). The mean annual growth rate of CH<sub>4</sub> decreased from 14 ~~ppb~~ ppbv/yr in 1984 to near zero in 1999 (Dlugokencky et al., 2003). From 1999 to 2006, globally averaged CH<sub>4</sub> was relatively constant but atmospheric methane concentrations started rising again in 2007 with a global average growth of ~6 ~~ppb~~ ppbv/year (Nisbet et al., 2014). Latest analysis by Saunois et al. (2016) suggests that the cause of the atmospheric growth trend of the past decade is predominantly biogenic - most likely from agriculture -  
15 with smaller contributions from fossil fuel use and possibly wetlands.

Our current understanding of the natural and anthropogenic emissions of CH<sub>4</sub> is insufficient. Although the global OH sink of CH<sub>4</sub> and the sum of CH<sub>4</sub> sources is relatively well known, there are still large uncertainties about each of the individual sources of CH<sub>4</sub>. However, due to its relatively short lifetime, it is now recognized that one of the most efficient methods to mitigate warming due to greenhouse gases on decadal time frames is to cut CH<sub>4</sub> emissions (Shindell et al., 2012). Global monitoring of  
20 CH<sub>4</sub> is therefore essential to increase our knowledge on how the different sources and sinks influence the atmospheric abundance of methane.

Atmospheric CH<sub>4</sub> has been measured continuously from space since 2003. Jacob et al. (2016) gives an extensive overview of past and future satellite missions dedicated to detect methane. Atmospheric CH<sub>4</sub> is detectable by its absorption of radiation in the shortwave infrared (SWIR) and thermal infrared (TIR). SWIR instruments, such as SCIAMACHY (Frankenberg et al.,  
25 2006), TANSO-FTS (Kuze et al., 2016) and the soon to be launched TROPOMI instrument (Hu et al., 2016), measure the solar radiation backscattered by the Earth and the atmosphere, and give a total atmospheric column of CH<sub>4</sub> with near uniform sensitivity in the troposphere (Jacob et al., 2016). TIR instruments measure the thermal radiation emitted by the Earth and the atmosphere, and operate in a nadir, limb or solar occultation observing mode. Limb and solar occultation detect CH<sub>4</sub> vertical profiles in the stratosphere and upper troposphere (Jacob et al., 2016). TIR nadir measurements provide integrated CH<sub>4</sub> columns in the  
30 middle to upper troposphere and allow day and nighttime concentrations, over land and sea. Examples are the AIRS instrument onboard the NASA Aqua satellite which has been providing global methane observations since 2002 (Xiong et al., 2008), TES which was operational from 2004 to 2011 (Worden et al., 2012), and IASI, launched onboard METOP-A MetOp-A in October 2006 and on METOP-B MetOp-B in September 2012 (~~Razavi et al., 2009; Crevoisier et al., 2009; Xiong et al., 2013~~) (Razavi et al., 2009;

With the launch of MERLIN foreseen in 2021, for the first time, active measurements will be made from space with an  
35 IPDA (Integrated Path Differential Absorption) LIDAR-lidar (Light Detecting And Ranging), which will provide atmospheric

methane columns with high precision and unprecedented accuracy on a global scale (Pierangelo et al., 2016).

As mentioned in the previous paragraph, in addition to the IASI CH<sub>4</sub> product presented here, other IASI CH<sub>4</sub> products exist. Crevoisier et al. (2009) uses a non-linear inference scheme based on neural networks, to derive a mid-tropospheric CH<sub>4</sub> column with peak sensitivity at about 230 hPa (~11 km), half the peak sensitivity at 100 and 500 hPa (~6 and 16 km), and no sensitivity to the surface. This dataset was previously only available for the tropical region between 30°S and 30°N but got extended to higher latitudes and is available through the Climate Change Initiative-Greenhouse Gas (CCI-GHG) project. The retrieval schemes of Siddans et al. (2016) and García et al. (2017) are based on the optimal estimation method (OEM), like the BIRA-IASB product. Different constraint matrices are used by the 2 products. García et al. (2017) et al use a Tikhonov-Philips slope constraint with strong regularisation (almost equivalent to a scaling retrieval). Siddans et al. (2016) use an a priori covariance matrix which describes the presumed errors in the a priori estimate of CH<sub>4</sub>. The IASI CH<sub>4</sub> product presented in this paper follows a similar approach as Siddans et al. (2016).

In this paper, we present a new CH<sub>4</sub> product retrieved from IASI radiances with the ASIMUT-ALVL software developed at BIRA-IASB. This product complements the BIRA-IASB height-resolved IASI aerosol dust product (Vandenbussche et al., 2013). Sect. 2 introduces the IASI mission. In Sect. 3 we describe the IASI CH<sub>4</sub> radiative transfer and the retrieval setup, and the use of the Principal Component Compressed IASI spectra is addressed. The information content of the IASI CH<sub>4</sub> product is presented in Sect. 4. In addition, global distributions are shown and retrieval processing details are briefly discussed. In Sect. 5 the IASI CH<sub>4</sub> product is compared to ground-based measurements, providing an quality assessment of the retrieved BIRA-IASB CH<sub>4</sub> columns. The final section summarizes the main results of this work and discusses future work.

## 2 IASI

The Infrared Atmospheric Sounding Interferometer (IASI) onboard ~~MetOp~~, ~~MetOp-A~~ is a thermal cross-nadir scanning infrared sounder. Launched in October 2006, it is the first in a ~~successive~~ series of three, together programmed to provide measurements for a period of 15 years. The second instrument onboard MetOp-B was launched in September 2012 and the launch of MetOp-C is scheduled for October 2018.

IASI is a Fourier Transform Infrared (FTIR) spectrometer which measures the TIR radiation emitted by the Earth and the atmosphere. With a wide swath width of 2 x 1100 km it provides near-global coverage twice a day, with a local overpass time at ~9:30 AM and PM. It has an instantaneous field of view (FOV) at nadir with a spatial resolution of 50 km x 50 km, composed of 2 x 2 circular pixels, each corresponding to a 12 km diameter footprint on the ground at nadir (Clerbaux et al., 2009). IASI has ~~four~~ ~~three~~ spectral bands in the spectral range from 645 to 2760 cm<sup>-1</sup> (3.62 to 15.5 μm), provided as a continuous spectrum with an apodized spectral resolution of 0.5 cm<sup>-1</sup> and spectral sampling of 0.25 cm<sup>-1</sup>.

Designed to provide highly accurate temperature and humidity profiles for numerical weather ~~predictions~~ prediction, the IASI mission allows simultaneous global observations of the air composition with an excellent spatial resolution. From the atmospheric spectra recorded by the instrument, concentrations of several trace gases can be monitored, enhanced levels of pollution can be detected, and particle types can be determined to some extent. ~~On~~ ~~In~~ the longer term the continuity of the

~~program-programme~~ is ensured with the IASI-NG mission that will extend the IASI ~~observation-observations~~ for 15-20 more years (Clerbaux et al., 2016).

### 3 The IASI CH<sub>4</sub> retrieval method

The IASI CH<sub>4</sub> profiles are retrieved with the ASIMUT-ALVL software developed at BIRA-IASB (Vandaele et al., 2006). ASIMUT-ALVL is a modular software for radiative transfer (RT) calculations and inversions in planetary atmospheres. The code has been developed with the objective to be as general as possible, accepting different instrument types and different geometries. ASIMUT-ALVL has been coupled to the SPHER/TMATRIX (Mishchenko and Travis, 1998) and LIDORT (Spurr, 2006) codes to include the complete treatment of the scattering effects into the RT calculations. It has a specific interface dealing with the IASI instrument characteristics and IASI input information and is also used for the IASI aerosol dust retrievals (Vandenbussche et al., 2013). The RT simulations are performed with the ASIMUT-ALVL RT code for the IASI CH<sub>4</sub> data product while the LIDORT RT code is used for the IASI aerosol dust retrievals in order to include all scattering effects due to aerosols. Both IASI retrieval products use the same retrieval module, based on the formalism of the ~~Optimal Estimation Method (OEM)-OEM~~ (Rodgers, 2000).

Initially developed for Earth observation missions, ASIMUT-ALVL has also been adapted for planetary atmospheres, in particular those of Venus (Vandaele et al., 2008) and Mars (Drummond et al., 2011) and is now the reference code for the NOMAD instrument ~~on-board-onboard~~ ExoMars TGO (Robert et al., 2016).

#### 3.1 Forward model

The ASIMUT-ALVL RT module simulates atmospheric transmittances and radiances for cases under local thermodynamical equilibrium and where scattering can be neglected. A detailed description of the radiative transfer model is given in Vandaele et al. (2006). The spectral range considered for the CH<sub>4</sub> retrieval is the 1210-1290 cm<sup>-1</sup> ~~range-region~~ covering part of the  $\nu_4$  spectral band. EUMETSAT IASI L2 ~~temperature-skin temperature (T<sub>skin</sub>), temperature~~ and water vapour profiles are used as input for the radiative transfer calculations. The spectroscopic parameters for CH<sub>4</sub>, N<sub>2</sub>O and other species are taken from the HITRAN 2012 database (Rothman et al., 2013). The IASI Instrument Line Shape (ILS) is characterized by a Gaussian function with a 0.5 cm<sup>-1</sup> FWHM. Frequency dependent emissivity maps are provided by Zhou et al. (2011). Fig. 1 shows an example of measured and simulated radiances in the 1210-1290 cm<sup>-1</sup> spectral ~~range-and-its-region and the~~ residual (difference between measured and simulated radiances). ~~We have a~~ In the lower panel, the overlapping contributions of the different molecules CH<sub>4</sub>, H<sub>2</sub>O and N<sub>2</sub>O are illustrated. Here the radiances are simulated under the assumption of a single-species atmosphere containing either CH<sub>4</sub>, H<sub>2</sub>O or N<sub>2</sub>O. The top panel shows a negligible bias and a 1- $\sigma$  standard deviation comparable to the radiometric noise of  $2 \times 10^{-8}$  W/(cm<sup>2</sup> sr cm<sup>-1</sup>) (see Sect. 3.2). Certain spectral ranges in the considered spectral ~~band-region~~ are not well simulated by the radiative transfer model, leading to outliers in the residuals with absolute differences larger than  $5 \times 10^{-8}$  W/(cm<sup>2</sup> sr cm<sup>-1</sup>), for example at 1246 cm<sup>-1</sup> and 1252 cm<sup>-1</sup>. These spectral ranges are masked in the retrieval set-up, i.e. the ~~radiometric-noise-signal-to-noise~~ is set to zero at these spectral points, so that no information is lost.

Only IASI L1C spectra with a cloud fraction  $< 10\%$  based on the EUMETSAT IASI L2 fractional cloud cover product are processed.

### 3.2 Retrieval and error characterization

The ASIMUT retrieval module is based on the OEM (Rodgers, 2000) where the Jacobians are calculated analytically. The characteristics of the IASI retrieval are summarized in Table 1. The state vector includes ~~the skin temperature~~ ( $T_{\text{skin}}$ ), 23-level  $\text{CH}_4$ ,  $\text{N}_2\text{O}$  and  $\text{H}_2\text{O}$  profiles and a  $\text{CO}_2$  total column. The  $T_{\text{skin}}$  a priori is taken from the EUMETSAT IASI L2  $T_{\text{skin}}$  product. The a priori profiles  $x_a$  and covariance matrices  $S_a$  for  $\text{CH}_4$  and  $\text{N}_2\text{O}$  are based on a climatology from the WACCM model. ~~The A single global  $\text{CH}_4$   $x_a$  profile is used for all the retrievals, representative of a mid-latitude  $\text{CH}_4$  profile. Therefore the atmospheric  $\text{CH}_4$  variations observed are a results of the variability of atmospheric  $\text{CH}_4$  rather than the a priori information.~~  
10 ~~The  $\text{CH}_4$  covariance matrix represents the highest variability at the surface and in the upper troposphere-lower stratosphere (UTLS). The variability in the UTLS is representative for the variability of the  $\text{CH}_4$  gradient at the tropopause which is different at different latitudes.~~ The  $\text{H}_2\text{O}$  a priori uncertainty covariance matrix is characterised by an uncertainty covariance matrix with a 10% standard deviation on the diagonal and an exponential decaying correlation width of 6 km. The EUMETSAT IASI L2 water vapour profile is used as the  $\text{H}_2\text{O}$  a priori profile  $x_a$ . The interfering species  $\text{HNO}_3$  and  $\text{O}_3$  are included in the RT  
15 calculations, ~~its~~ ~~their~~ a priori values are provided by the WACCM model.

A diagonal measurement uncertainty covariance  $S_e$  is taken, with the radiometric noise set to  $2 \times 10^{-8} \text{ W}/(\text{cm}^2 \text{ sr cm}^{-1})$ . This value is conservative, about a factor 5 higher than the estimated radiometric noise in this spectral region of  $4 \times 10^{-9} \text{ W}/(\text{cm}^2 \text{ sr cm}^{-1})$  (Clerbaux et al., 2009). It includes not only the measurement uncertainty, but also the uncertainties in the temperature and water ~~vapor~~ ~~vapour~~ profile, the spectroscopic parameters and surface emissivity (De Wachter et al., 2012).

20 Fig. 2 presents the  $\text{CH}_4$  a priori profile (pink) and retrieved  $\text{CH}_4$  profile (blue) in volume mixing ratio (vmr) for a pixel at  $27^\circ\text{N}$ . The horizontal bars represent the retrieval uncertainty. The averaging kernel (AK) is given in the middle figure. It shows that the sensitivity of the IASI  $\text{CH}_4$  product lies in the 800-100 hPa ( $\sim 2$ -16 km) range. The right plot of Fig. 2 ~~diplays~~ ~~displays~~  
the vertical profiles of the retrieval uncertainties together with the  $\text{CH}_4$  a priori variability (black line). The square root of the diagonal elements of the uncertainty is plotted. The  $\text{CH}_4$  a priori variability is calculated from the square root of the diagonal of  
25 the a priori uncertainty covariance matrix. The retrieval is quite constrained with ~~of~~ an a priori variability of a few percent at the surface going up to 7-8% at 20 km. Following Rodgers (2000) the error sources contributing to the total retrieval uncertainty are 1) the smoothing error, which accounts for the vertical resolution of the retrieved  $\text{CH}_4$ , 2) the error due to uncertainties in forward model parameters such as spectroscopy, the temperature profile, surface emissivity and 3) the IASI measurement uncertainty. For IASI the forward model uncertainties are included in the measurement uncertainty. As we can see from Fig.  
30 2, the dominant source of uncertainty is the smoothing uncertainty. The total retrieval uncertainty declines from 3% at the ~~su~~ ~~rface~~ ~~surface~~ to  $\sim 2\%$  between 800 and 200 hPa, the altitude range of maximum sensitivity. Above 200 hPa the total retrieval uncertainty increases rapidly up to  $\sim 4\%$  at 100 hPa and  $\sim 6\%$  at 60 hPa.

### 3.3 Retrievals with PCC L1C data

The CH<sub>4</sub> profiles are retrieved from IASI radiances recomposed from the EUMETSAT Principal Component Compressed (PCC) L1C dataset (Hultberg, 2009). The use of PCC data allows both noise filtering and a large reduction in data volume compared to the use of raw radiances. Our main motivation is the large reduction in data storage. One year of the original IASI L1C (BUFR format) data amounts to 10 Tb which is reduced to 1 Tb /year for the PCC data. Fig. 3 shows the raw and PCC radiances for a random pixel in the CH<sub>4</sub> ν<sub>4</sub> spectral band. Differences between raw radiances and PCC radiances lie in the IASI radiometric noise level ( $4 \times 10^{-9} \text{ W}/(\text{mcm}^2 \text{ sr mcm}^{-1})$ ) as given by the IASI radiometric noise figure from Clerbaux et al. (2009). This is a factor 5 lower than the conservative radiometric noise level of  $2 \times 10^{-8} \text{ W}/(\text{mcm}^2 \text{ sr mcm}^{-1})$  used in the CH<sub>4</sub> retrieval (see Sect. 3.1). Fig. 4 compares the CH<sub>4</sub> concentrations retrieved with the PCC L1C data with those retrieved with the raw radiances for March 2011 and September 2013 for daytime and nighttime retrievals between 60°S and 70°N. We find an excellent correlation (R=1) between the retrieved concentrations and negligible biases of 0.0026% and 0.025% with a 1-σ standard deviation of  $\leq 0.12\%$ . With these results we are confident to use the PCC-reconstructed radiances.

## 4 The BIRA-IASB IASI CH<sub>4</sub> product

### 4.1 Information content

For correct interpretation of the data one needs to consider the vertical sensitivity of the retrieved CH<sub>4</sub> profile. This information is contained in the averaging kernel (AK), which is provided with each retrieved CH<sub>4</sub> profile. The peak of each AK gives the altitude of maximum sensitivity. Its full width at half maximum can be interpreted as the vertical resolution of the retrieval. Averaging kernels are variable, as can be seen from Fig. 5. Given is the CH<sub>4</sub> AK for 3 pixels in March 2013 at 3 different geographical locations; at northern mid-latitudes (55-52 °N), in the tropics (4 °N) and at southern mid-latitudes (47 °S). In the tropics, the CH<sub>4</sub> sensitivity lies in the 850-100 hPa (~1.5-16 km) range, at mid-latitudes, in the 700-200 hPa (~3-12 km) range. For the 3 geographical locations, the sensitivity is reduced in the boundary layer, which is typical for thermal infrared sounders. In each figure the Degree of Freedom for Signal (DOFS) is given, which is an estimate of the number of independent pieces of information contained in the measurement. It is the trace of the AK. One independent piece of information ( $1.04 < \text{DOFS} < 1.47$ ) is deduced for the 3 geographical locations. Maps of the CH<sub>4</sub> DOFS for February and August 2013 are presented in Fig. 6. DOFS values for daytime retrievals are shown in the 2 lefthand figures, DOFS values for nighttime retrievals are shown in the 2 righthand figures. For both seasons and day- or nighttime retrievals we typically have DOFS values in the tropics around 1.4. For the Northern Hemisphere (NH), at mid-latitudes, we see higher DOFS values in August (NH summer) than in February (NH winter). In February values can become less than 1 for latitudes  $> 40^\circ\text{N}$ . The variability of the AK (and hence the DOFS) is dependent on the thermal contrast (the difference between the surface temperature and the temperature of the first atmospheric vertical layer), which exhibits significant geographical, seasonal, and diurnal variability. The retrieval sensitivity is favourable, and hence the DOFS is high, when thermal contrast is high. In general the thermal contrast or the DOFS is higher during the day, over land, and over dry, sparsely vegetated regions (Clerbaux et al., 2009). This

pattern is visible in Fig. 6, where DOFS values are generally higher for daytime retrievals compared to the nighttime retrievals, and where high DOFS values are found for the daytime observations at desert regions of Africa and Australia. The DOFS for different latitudinal bands for February and August 2013 is presented in Fig. 7. DOFS values for daytime retrievals are provided in the 2 lefthand figures, DOFS values for nighttime retrievals are shown in the 2 righthand figures. This figure confirms that

5 DOFS values in the tropics are typically around 1.4. For August (NH summer), on the global scale, the DOFS values for daytime retrievals range between 1 and 1.8 (between 0.9 and 1.6 for nighttime retrievals). For February (NH winter), values range between 0.4 and 1.7 (between 0.4 and 1.6 for nighttime retrievals), when values can become less than 1 for latitudes  $> 40^{\circ}\text{N}$ . So overall one independent piece of information is retrieved with a good sensitivity in the mid to upper troposphere.

## 4.2 Global distributions

10 Monthly mean global daytime distributions for the year 2013 are presented in Fig. 8. IASI  $\text{CH}_4$  partial columns between 4 and 17 km between  $60^{\circ}\text{S}$  and  $70^{\circ}\text{N}$  are shown for the IASI morning overpass.  $\text{CH}_4$  concentrations are averaged over the four,  $2 \times 2$  circular IASI pixels, which are measured simultaneously (see Sect. 2) and binned on a  $1^{\circ} \times 1^{\circ}$  grid. Areas with missing data correspond to areas which were identified as cloudy by the EUMETSAT IASI L2 fractional cloud cover product, or correspond to areas where not all of the 4 simultaneously measured pixels converged in the retrieval.

15 We see a latitudinal gradient with higher concentrations in the Northern Hemisphere (NH) than in the Southern Hemisphere (SH), which is consistent with the fact that most of the methane sources are located in the Northern Hemisphere. In the NH, higher  $\text{CH}_4$  concentrations are found during boreal summer than during boreal winter. This summer increase of mid to upper tropospheric  $\text{CH}_4$  has also been observed by AIRS (Xiong et al., 2010). Van Weele et al. (2011) examined the  $\text{CH}_4$  variability in the upper troposphere and lower stratosphere between  $\sim 6\text{-}25$  km using aircraft observations and the TM5-chem-

20 v3.0 chemistry transport model (Krol et al., 2005; Huijnen et al., 2010). They also found higher  $\text{CH}_4$  mixing ratios at the 500 hPa level ( $\sim 6$  km) at high latitudes during boreal summer compared to winter concentrations and attributed the winter minimum to enhanced downward transport from the stratosphere.

Methane observed in the boundary layer by surface stations from the NOAA network displays a reversed seasonal cycle in the NH (Dlugokencky et al., 2009). These results demonstrate the added value of thermal infrared  $\text{CH}_4$  measurements which have

25 a sensitivity at higher altitudes.

## 4.3 Error analysis

In Sect. 3.2 we discussed the two error sources which contribute to the total retrieval error: the smoothing error, which accounts for the low vertical resolution of the retrievals, and the measurement error. Their uncertainties are estimated following Rodgers (2000) and are shown in Fig. 2. Additional sources of error propagating into the total retrieval error are due to

30 uncertainties in forward model parameters or ancillary data used in the inversions. These error sources are currently not explicitly taken into account in the ASIMUT retrieval software. We therefore estimated the uncertainties by forward model parameters or ancillary data by a perturbation method, following Barret et al. (2002, 2003) . A set of spectra in a latitude-longitude band between  $60^{\circ}\text{S}$ - $70^{\circ}\text{N}$  and  $120$ - $125^{\circ}\text{E}$  were selected, comprising a set of 4000 spectra. This is a representative set for the

latitudinal coverage of the IASI CH<sub>4</sub> dataset, with spectra over land and water. For the different error sources considered, IASI CH<sub>4</sub> is retrieved for this set of spectra with the original set-up and the uncertainty added to the specific error source. The uncertainty of this error source on the IASI CH<sub>4</sub> partial column is then estimated as the difference between the newly retrieved IASI CH<sub>4</sub> partial column (with the uncertainty of the error source added) and the IASI CH<sub>4</sub> partial column from the current optimized retrieval set-up. The different error sources and their uncertainties are listed in Table 2, as well as the results of the estimated uncertainties of the IASI CH<sub>4</sub> 4-17 km partial column for each individual error source.

The uncertainty of the temperature profile on the CH<sub>4</sub> partial column is estimated by substituting the IASI L2 temperature profiles with the ECMWF ERA-Interim (Dee et al., 2011) re-analysis temperature profiles. ECMWF ERA-Interim re-analysis data is available at 6 hourly intervals with a horizontal resolution of  $\sim 0.75^\circ$  in latitude and longitude. The temperature profiles are interpolated to the location and time of the IASI pixel and the retrieved CH<sub>4</sub> is compared with the CH<sub>4</sub> partial column of the optimized retrieval set-up. For the CH<sub>4</sub> absorption lines the uncertainty on the line intensity, the air and self broadening coefficients is set to 2%. This is consistent with what García et al. (2017) considered in their uncertainty estimation. For the interfering species, N<sub>2</sub>O, H<sub>2</sub>O and isotopologues, which are simultaneously retrieved, we also set the uncertainties on the spectroscopic parameters (line intensity and air and self broadening coefficients) to 2%. We also estimated a systematic uncertainty of the IASI CH<sub>4</sub> a priori of 2%. Following García et al. (2017) the uncertainty on the emissivity is 1% for all wavenumbers. For the PCC uncertainty we calculated the difference between IASI CH<sub>4</sub> retrieved from PCC spectra and from raw spectra, as already shown in Sect. 3.3. The smoothing and measurement uncertainty are estimated as in Sect. 3.2.

The third column in Table 2 lists the results. The dominant sources of error are the smoothing error and the CH<sub>4</sub> line intensity with an uncertainty on the IASI CH<sub>4</sub> 4-17 km partial column of 2.45% and 1.93% respectively. Other error sources contributing significantly to the uncertainty of the CH<sub>4</sub> 4-17 km partial column are the temperature profile (1.40%), the CH<sub>4</sub> broadening coefficients (1.09%) and the measurement uncertainty (0.95%). There is also a non-negligible contribution of the emissivity uncertainty of 0.27%. Uncertainties in the spectroscopic parameter of N<sub>2</sub>O, H<sub>2</sub>O and its isotopologues do not significantly contribute to the uncertainty in CH<sub>4</sub>. The systematic uncertainty of the IASI CH<sub>4</sub> a priori also has a negligible effect of 0.06%. Combining the different contributions to the IASI CH<sub>4</sub> error budget, we estimated a total uncertainty on the CH<sub>4</sub> 4-17 km partial column of 3.73%. If we consider the temperature, measurement, PCC reconstruction and smoothing uncertainty as random error sources we get an estimate of the precision of the IASI CH<sub>4</sub> 4-17 km partial column of 2.98%. If we consider uncertainties in the spectroscopy and emissivity as systematic error sources, the systematic uncertainty of the CH<sub>4</sub> 4-17 km partial column is 2.23%.

#### 4.4 Retrieval output and processing

The BIRA-IASB IASI CH<sub>4</sub> product is delivered in HDF5 format. Daily daytime and nighttime observations are provided in separate files. The HDF files contain CH<sub>4</sub> profiles, the retrieval uncertainty, the CH<sub>4</sub> a priori profiles and averaging kernels. BIRA-IASB entered Phase 2 of the ~~Climate Change Initiative-Greenhouse Gas (CCI-GHG)~~ project (Buchwitz et al., 2015) and a dataset has been generated for the years 2011-2014, contributing to Climate Research Data Package No.4 (CRDP#4). These retrievals were performed between 60°S and 70°N and can be downloaded from <http://iasi.aeronomie.be/>. Data is processed

on a High Performance computing system (HPC) with 2 x 55 nodes of 24 Central Processing Units (CPUs) where the user obeys a quota-based use. One day of IASI CH<sub>4</sub> data (for the 60°S and 70°N region) is processed in 48 hours on 1 node with 24 CPUs.

## 5 Validation

5 Ground-based data was collected from 10 FTIR stations from the Network for the Detection of Atmospheric Composition Change (NDACC). The stations chosen are operated on a quasi-continuous basis and deliver CH<sub>4</sub> vertical profiles. Certain stations provide limited observations since they only recently entered the NDACC network or since they only make campaign measurements. We therefore excluded stations with ~~less~~-fewer than 200 collocations due to insufficient collocation points for a statistically significant comparison. NDACC FTIR CH<sub>4</sub> profiles have good sensitivity in the troposphere and stratosphere  
 10 with 2 to 3 independent pieces of information. Note, the NDACC CH<sub>4</sub> retrieval is not fully harmonized yet for all the NDACC stations. This work is ongoing as part of the Horizon 2020 Gap Analysis for Integrated Atmospheric ECV CLimate Monitoring (GAIA-CLIM) project (<http://www.gaia-clim.eu/>).

We performed a detailed comparison between IASI and NDACC CH<sub>4</sub> partial columns between 4 and 17 km at these 10 NDACC stations for the period 2011 to 2014. Since the two retrievals have been computed with a different a priori, the  
 15 NDACC retrieved profiles are adjusted for the comparison. Following [Roggers and Connor \(2003\)](#) (equation 10), the term  $(\mathbf{A}_{\text{NDACC}} - \mathbf{I}) \cdot (\mathbf{x}_{\text{a,NDACC}} - \mathbf{x}_{\text{a,IASI}})$  is added to each NDACC retrieval to adjust for the different a priori profile used in the IASI retrieval. Here  $\mathbf{A}_{\text{NDACC}}$  is the NDACC averaging kernel,  $\mathbf{I}$  the unity matrix,  $\mathbf{x}_{\text{a,NDACC}}$  the NDACC CH<sub>4</sub> a priori profile and  $\mathbf{x}_{\text{a,IASI}}$  the IASI CH<sub>4</sub> a priori profile.

In addition, to account for the different resolution between the IASI and the higher resolved NDACC FTIR profiles, a smoothing  
 20 is applied to the (a priori adjusted) NDACC profile  $\mathbf{x}_{\text{NDACC}}$  by the IASI averaging kernel:

$$\hat{\mathbf{x}}_{\text{NDACC}} = \mathbf{x}_{\text{a,IASI}} + \mathbf{A}_{\text{IASI}} \cdot (\mathbf{x}_{\text{NDACC}} - \mathbf{x}_{\text{a,IASI}}) \quad (1)$$

where  $\hat{\mathbf{x}}_{\text{NDACC}}$  is the smoothed or convolved NDACC CH<sub>4</sub> profile and  $\mathbf{x}_{\text{a,IASI}}$  and  $\mathbf{A}_{\text{IASI}}$  are the IASI a priori profile and averaging kernel.

From the IASI and smoothed NDACC CH<sub>4</sub> profiles partial columns are calculated between 4 and 17 km. The average is taken  
 25 of IASI pixels selected within 3 hours of the NDACC FTIR measurement, in a 0.5°-1.5° latitude-longitude-box centred around the point on the line of sight (LOS) where the FTIR measurement has maximum sensitivity (typically at 5km ~~altitude~~-altitude on the LOS). To guarantee a certain homogeneity of the NDACC data with NDACC CH<sub>4</sub> profiles of comparable quality we applied a filtering on some of the NDACC data when large outliers where found. We also applied a filtering to the IASI CH<sub>4</sub> profiles. We omitted IASI pixels with DOFS<0.85 and when the root mean square of the residual>2.2x10<sup>-8</sup> W/(cm<sup>2</sup> sr cm<sup>-1</sup>).

30

Fig. 9 summarizes the results in a bar chart giving the relative difference between IASI and smoothed NDACC partial columns between 4 and 17 km at the different NDACC stations. The relative mean difference  $\Delta=(\text{IASI-NDACC})/\text{NDACC}$  and standard

deviation of the difference ( $\sigma$ ) in percentage is given for each station. Relative mean differences between IASI and NDACC lie between ~~-1.93 and 0.67~~ -2.31 and 0.18% (of which ~~7~~ 6 stations out of 10 less than  $\pm 1\%$ ) with exception of the Thule station, where IASI is biased high with respect to NDACC by 4.44.04%. The standard deviation of the difference lies in the range ~~1.91 to 3.99~~ 1.76 to 2.97% for the 10 stations.

- 5 It is important to compare these results with the uncertainty budget of the IASI and the NDACC CH<sub>4</sub> partial columns. As given by ~~?~~ Rodgers and Connor (2003) (equation 30),  $S_{\Delta}$ , the covariance of the difference IASI-NDACC, can be calculated as:

$$S_{\Delta} = (A_{IASI} - A_{IASI}A_{NDACC})S_{a,IASI}(A_{IASI} - A_{IASI}A_{NDACC})^T + S_{IASI} + A_{IASI}S_{NDACC}A_{IASI}^T$$

- 10 The first term is the smoothing uncertainty of the comparison ensemble (the smoothed and a priori-corrected NDACC and IASI product) with  $S_{a,IASI}$  the IASI a priori uncertainty covariance matrix.  $S_{IASI}$  is the IASI retrieval uncertainty covariance excluding the smoothing uncertainty and  $S_{NDACC}$  is the NDACC retrieval uncertainty covariance without the smoothing uncertainty. We compare the systematic and random uncertainty on the difference directly to the mean difference and standard deviation of the difference between IASI and NDACC. NDACC provides systematic and random uncertainty covariances for the different
- 15 stations, with exception of Jungfraujoch. For IASI we set the random uncertainty  $S_{a,IASI}^{rand}$  equal to the IASI a priori uncertainty covariance matrix used in the IASI retrieval. We calculated a systematic component  $S_{a,IASI}^{syst}$  with a 2% standard deviation of the a priori profile values. Separating the systematic and random component of  $S_{IASI}$  is less straightforward. Here we only consider the IASI measurement uncertainty as the random uncertainty and we do not consider the systematic component.

- Table 3 lists the results of this analysis with the relative mean differences, the standard deviation of the differences and the
- 20 mean values of the systematic and random uncertainties. We have a good agreement where the IASI-NDACC mean differences lie within the systematic uncertainty. Also for Thule the mean difference of 4.404.04% is within the systematic uncertainty of 5.145.28%. The standard deviation of the difference is ~~close to~~ within the random uncertainty, ~~but for certain stations slightly larger. This discrepancy could be due to an additional error associated with the grid conversions or a geolocation error which are not taken into account (Calisesi et al., 2005; Vigouroux et al., 2009).~~ Another reason could be the ~~for all stations. We did~~ notice a current underestimation of the random uncertainty of the NDACC CH<sub>4</sub> retrievals. They were found to be less than 1% for 6 out of the 10 NDACC stations. Also note the spread in uncertainty estimates, especially for the systematic component. This is due to the differences in reported systematic and random error covariances from the different NDACC stations. The ongoing work in the GAIA-CLIM project will harmonize the error characterization for all NDACC stations in the coming period. This comparison stresses the importance of this harmonization work.

- 30 Scatter plots of collocated partial columns are presented in Fig. 10. We find ~~very~~ good correlations ( $R =$ ~~0.71-0.88~~ 0.67-0.84) for the **high-latitude** stations Eureka, Thule and Kiruna. ~~High correlations ( $R > 0.9$ )~~ Good correlations are found as well for the **mid-latitude** stations Jungfraujoch ~~and Zugspitze ( $R = 0.81$ ) and Zugspitze ( $R = 0.68$ )~~, while the mid-latitude ~~stations~~ station Toronto performs poorer with a correlation of 0.440.52. The **tropical** island stations Izaña, Maito and Mauna Loa show poor correlations ( $R =$ ~~0.41-0.50~~ 0.15-0.37) although biases are below 11.20% for these stations. ~~The tropical island station Izaa~~

~~however shows a high correlation of 0.90.~~ For the most Southern station Wollongong (34°S) we find a ~~good correlation of~~ 0.77. ~~The poorer correlations at the Mauna Loa, Maito and Toronto stations could be attributed~~ correlation of 0.60. Several tests were performed to explain the poorer correlations found at the tropical island stations. We applied a stronger filtering on the IASI and NDACC data but found no improvement. We investigated a possible relation of IASI land or IASI sea pixels with differences between the IASI and NDACC retrieved CH<sub>4</sub> but found no correlation. We therefore attribute the poorer correlations at the Izaña, Mauna Loa and Maito stations to the lower CH<sub>4</sub> variability we see at these locations compared to the other stations. In addition, at ~~Mauna Loa and Toronto~~ Maito and Mauna Loa, we see a few outliers which could explain the poorer linear regression fit at these stations. ~~These results demonstrate the ability of the IASI data to well capture the temporal variation of CH<sub>4</sub>.~~

## 6 Discussion, conclusion and outlook

Although CH<sub>4</sub> is a more effective greenhouse gas than CO<sub>2</sub>, it has a much shorter atmospheric lifetime than CO<sub>2</sub> that can remain in the atmosphere for hundreds or thousands of years. Therefore the mitigation of CH<sub>4</sub> emissions provides an opportunity for alleviating climate change in the short-term future (Kirschke et al., 2013). Global monitoring of CH<sub>4</sub> is essential to study the evolution of atmospheric CH<sub>4</sub> and to help increase our knowledge on how the different sources and sinks influence its atmospheric abundance.

In this paper, we presented a new IASI CH<sub>4</sub> retrieval product developed at BIRA-IASB. Global distributions of CH<sub>4</sub> were derived from IASI radiances with the ASIMUT-ALVL software based on the OEM. A detailed description of the forward model, the retrieval strategy and the use of PCC LIC data was given. CH<sub>4</sub> concentrations retrieved from raw radiances and PCC-reconstructed radiances showed an excellent correlation and negligible mean differences of < 0.026% (< 0.46 ~~ppb~~ ppbv).

We presented the latitudinal distribution of the DOFS for different seasons. We showed that, between 60°S and 70°N, the DOFS values range between 1 (0.9) and 1.8 (1.6) for daytime (nighttime) retrievals for NH summer. In NH winter values can become less than 1 for latitudes > 40°N. In tropical scenes DOFS values are typically around 1.4, with a good sensitivity in the mid to upper troposphere.

A quality assessment of the retrieved IASI CH<sub>4</sub> product was given by a detailed comparison with ground-based FTIR observations recorded at 10 NDACC stations. The BIRA-IASB product was compared to smoothed NDACC FTIR CH<sub>4</sub> partial columns between 4 and 17 km for the years 2011 to 2014. We found a very good agreement between both products with differences within the systematic uncertainty. Mean difference values range between ~~-1.93 and 4.40~~ -2.31 and 4.04% for the 10 stations. Absolute differences are less than 1% for ~~7~~ 6 stations out of 10. The standard deviation of the difference lies in the range ~~1.91 to 3.99~~ 1.76 to 2.97% for all the stations. These values are ~~close to~~ within the random uncertainty of IASI and NDACC, ~~but for certain stations slightly larger. Possible reasons for this discrepancy could be an underestimation of the NDACC CH<sub>4</sub> random uncertainty or additional error sources not considered in the calculation of the random uncertainty, such as a regridding or geolocation error.~~ Very good correlations are found for ~~7~~ 6 out of the 10 NDACC stations with correlation coefficients between ~~0.71 and 0.96~~ 0.60 and 0.84. Particularly for the 3 high-latitude stations we find high correlations, as well

as for the 2 high-quality mid-latitude stations Jungfraujoch and Zugspitze. ~~With these results we are confident that the IASI data is capturing the mid to upper-~~

Sect. 1 highlighted the need to improve our current understanding of the global budget of CH<sub>4</sub>. The Requirements Baseline Document (RBD) of the CCI-Climate Modelling User Group (CMUG) stipulates the observational requirements for regional  
5 source/sink determination of CH<sub>4</sub>. The RBD states that a CH<sub>4</sub> profile/tropospheric CH<sub>4</sub> column observation at a horizontal resolution of 50 km requires a precision of 1% and an accuracy of 2% for a 6h observing cycle (CMUG-RBD, 2015). To reach these demanding requirements improvements in the precision of the IASI 4-17 km partial column are needed. The error analysis in Section 4.3 gives a random uncertainty of 2.98% with the largest contribution coming from the smoothing error and uncertainty of the temperature profile. The simultaneous retrieval of the temperature profile could improve the IASI precision  
10 and will be investigated in the near future. The systematic uncertainty estimate in Section 4.3 of 2.23% could be improved by reducing spectroscopic uncertainties. Continuous efforts will be made on improving the IASI CH<sub>4</sub> variability well retrievals as to these issues and enhancing their precision.

Future work will further focus on extending the validation with additional datasets. Validation measurements for atmospheric vertical profiles for CH<sub>4</sub> are limited and very diverse. An innovative atmospheric sampling system called AirCore (~~Karion et al., 2010; ?~~) (K  
15 been demonstrated to be a reliable concept to make vertical profile measurements of CO<sub>2</sub>, CH<sub>4</sub> and CO from the surface up to ~30 km. Although campaign-based, these high precision measurements provide a promising and novel validation tool. One of the next steps is to compare the IASI CH<sub>4</sub> with AirCore CH<sub>4</sub> profiles. Further, a global scale comparison with the neural network IASI-CH<sub>4</sub> product (Crevoisier et al., 2009) or with one of the new OEM IASI-CH<sub>4</sub> products recently published and under revision (Siddans et al., 2016; García et al., 2017) would be of particular interest.

20 IASI provides day- and nighttime measurements over land and sea and has a high spatial coverage. Its follow-up missions guarantee a long continuity of observations and its successor, the IASI-NG next-generation instrument, will ensure a continuity of data until after 2040. IASI-NG's spectral resolution and signal-to-noise ratio will be improved by a factor of two. It will fly on the three second-generation MetOp-SG-A series, scheduled to launch in 2021, 2028 and 2035. IASI provides therefore a great opportunity for continuous monitoring of the atmospheric composition on a fine spatio-temporal scale.

25 ~~CH<sub>4</sub> is a challenging component to retrieve in the thermal infrared. Water vapour interferes strongly in the CH<sub>4</sub> thermal band. The same holds for the greenhouse gas N<sub>2</sub>O which is strongly correlated to CH<sub>4</sub>. In addition, spectroscopic uncertainties and mixing of spectral lines are still important issues in the CH<sub>4</sub> ν<sub>4</sub> band. Continuous efforts will be made on improving the IASI CH<sub>4</sub> retrievals as to these issues and enhancing their precision.~~ Furthermore, future work will focus on comparing the IASI concentrations with tagged simulations of CH<sub>4</sub> to see whether the model output is supported by the IASI data. With this re-  
30 search we want to provide a better understanding of the CH<sub>4</sub> budget, which can help target the pertinent sources for reducing CH<sub>4</sub> emissions and the associated climate impact of this greenhouse gas.

The BIRA-IASB IASI CH<sub>4</sub> dataset is available through the European Space Agency (ESA) CCI-GHG project and can be downloaded from <http://iasi.aeronomie.be/>. Data is available for the years 2011-2014 between 60°S and 70°N and CH<sub>4</sub> profiles, a priori profiles, retrieval uncertainties and averaging kernels are provided.

*Acknowledgements.* The IASI mission is a joint mission of Eumetsat and the Centre National d'Etudes Spatiales (CNES, France). The IASI L1C data are distributed in near real time by Eumetsat through the Eumetcast system distribution. This work was conducted as part of the IASI.flow (Infrared Atmospheric Sounding with IASI and Follow-on missions) project, funded by the Belgian Science Policy Office and the European Space Agency (ESA-Prodex ~~program~~programme). Additional support was provided by the ESA ~~GHG-CCI~~CCI-GHG project through the Optional Workpackage 706 TIRS (CO<sub>2</sub> and CH<sub>4</sub> from Thermal Infrared Sounders: IASI and ACE-FTS). The ground-based data used in this publication were obtained as part of the Network for the Detection of Atmospheric Composition Change (NDACC) and are publicly available (see <http://www.ndacc.org>).

~~Buchwitz, M., M. Reuter, O. Schneising, H. Boesch, I. Aben, M. Alexe, R. Armante, P. Bergamaschi, H. Bovensmann, D. Brunner, B. Buchmann, J. P. Burrows, A. Butz, F. Chevallier, A. Chedin, C. D. Crevoisier, M. De Maziere, E. De Wachter, R. Detmers, B. Dils, C. Frankenberg, S. Gonzi, P. Hahne, O. P. Hasekamp, W. Hewson, J. Heymann, S. Houweling, M. Hilker, T. Kaminski, G. Kuhlmann, A. Laeng, T. T. v. Leeuwen, G. Lichtenberg, J. Marshall, S. Noel, J. Notholt, P. I. Palmer, R. Parker, P. Somkuti, M. Scholze, G. P. Stiller, T. Warneke, C. Zehner, THE GREENHOUSE GAS PROJECT OF ESA'S CLIMATE CHANGE INITIATIVE (GHG-CCI): PHASE 2 ACHIEVEMENTS AND FUTURE PLANS, ESA ATMOS 2015 conference proceedings (ESA SP-735), Heraklion, Greece, 8-12 June 2015, 2015.~~

## References

- Barret, B., De Mazière, M., and Demoulin, P.: Retrieval and characterization of ozone profiles from solar infrared spectra at the Jungfraujoch, *Journal of Geophysical Research: Atmospheres*, 107, <http://dx.doi.org/10.1029/2001JD001298>, 4788, 2002.
- Barret, B., De Mazière, M., and Mahieu, E.: Ground-based FTIR measurements of CO from the Jungfraujoch: characterisation and comparison with in situ surface and MOPITT data, *Atmospheric Chemistry and Physics*, 3, 2217–2223, <https://www.atmos-chem-phys.net/3/2217/2003/>, 2003.
- Buchwitz, M., Reuter, M., Schneising, O., Boesch, H., Aben, I., Alexe, M., Armante, R., Bergamaschi, P., Bovensmann, H., Brunner, D., Buchmann, B., Burrows, J. P., Butz, A., Chevallier, F., Chedin, A., Crevoisier, C. D., De Mazière, M., De Wachter, E., Detmers, R., Dils, B., Frankenberg, C., Gonzi, S., Hahne, P., Hasekamp, O. P., Hewson, W., Heymann, J., Houweling, S., Hilker, M., Kaminski, T., Kuhlmann, G., Laeng, A., v. Leeuwen, T. T., Lichtenberg, G., Marshall, J., Noel, S., Notholt, J., Palmer, P. I., Parker, R., Somkuti, P., Scholze, M., Stiller, G. P., Warneke, T., and Zehner, C.: THE GREENHOUSE GAS PROJECT OF ESA'S CLIMATE CHANGE INITIATIVE (GHG-CCI): PHASE 2 ACHIEVEMENTS AND FUTURE PLANS, ESA ATMOS 2015 conference proceedings (ESA SP-735), 2015.
- Calisesi, Y., Soebijanta, V. T., and van Oss, R.: Regridding of remote soundings: Formulation and application to ozone profile comparison, *Journal of Geophysical Research: Atmospheres*, 110, d23306, 2005.
- Clerbaux, C., Boynard, A., Clarisse, L., George, M., Hadji-Lazaro, J., Herbin, H., Hurtmans, D., Pommier, M., Razavi, A., Turquety, S., Wespes, C., and Coheur, P.-F.: Monitoring of atmospheric composition using the thermal infrared IASI/MetOp sounder, *Atmospheric Chemistry and Physics*, 9, 6041–6054, <https://www.atmos-chem-phys.net/9/6041/2009/>, 2009.
- Clerbaux, C., Coheur, P.-F., Bauduin, S., Boynard, A., Clarisse, L., Doniki, S., George, M., Hadji-Lazaro, J., Hurtmans, D., Lacour, J.-L., Ronsmans, G., Van Damme, M., Wespes, C., and Whitburn, S.: Tracking pollutants from space: 10 years of IASI satellite observation, IGAC 2016 Science Conference (International Global Atmospheric Chemistry), 2016.
- CMUG-RBD: Requirements Baseline Document, [http://ensembles-eu.metoffice.com/cmug/CMUG\\_PHASE\\_2\\_D1.1\\_Requirements\\_v0.6.pdf](http://ensembles-eu.metoffice.com/cmug/CMUG_PHASE_2_D1.1_Requirements_v0.6.pdf), 2015.
- Crevoisier, C., Nobileau, D., Fiore, A. M., Armante, R., Chédin, A., and Scott, N. A.: Tropospheric methane in the tropics – first year from IASI hyperspectral infrared observations, *Atmospheric Chemistry and Physics*, 9, 6337–6350, <https://www.atmos-chem-phys.net/9/6337/2009/>, 2009.
- De Wachter, E., Barret, B., Le Flochmoën, E., Pavelin, E., Matricardi, M., Clerbaux, C., Hadji-Lazaro, J., George, M., Hurtmans, D., Coheur, P.-F., Nedelec, P., and Cammas, J. P.: Retrieval of MetOp-A/IASI CO profiles and validation with MOZAIC data, *Atmospheric Measurement Techniques*, 5, 2843–2857, <https://www.atmos-meas-tech.net/5/2843/2012/>, 2012.
- Dee, D. P., Uppala, S. M., Simmons, A. J., Berrisford, P., Poli, P., Kobayashi, S., Andrae, U., Balmaseda, M. A., Balsamo, G., Bauer, P., Bechtold, P., Beljaars, A. C. M., van de Berg, L., Bidlot, J., Bormann, N., Delsol, C., Dragani, R., Fuentes, M., Geer, A. J., Haimberger, L., Healy, S. B., Hersbach, H., Hólm, E. V., Isaksen, I., Kållberg, P., Köhler, M., Matricardi, M., McNally, A. P., Monge-Sanz, B. M., Morcrette, J.-J., Park, B.-K., Peubey, C., de Rosnay, P., Tavolato, C., Thépaut, J.-N., and Vitart, F.: The ERA-Interim reanalysis: configuration and performance of the data assimilation system, *Quarterly Journal of the Royal Meteorological Society*, 137, 553–597, <http://dx.doi.org/10.1002/qj.828>, 2011.
- Dlugokencky, E. J., Houweling, S., Bruhwiler, L., Masarie, K. A., Lang, P. M., Miller, J. B., and Tans, P. P.: Atmospheric methane levels off: Temporary pause or a new steady-state?, *Geophysical Research Letters*, 30, <http://dx.doi.org/10.1029/2003GL018126>, 1992, 2003.

- Dlugokencky, E. J., Bruhwiler, L., White, J. W. C., Emmons, L. K., Novelli, P. C., Montzka, S. A., Masarie, K. A., Lang, P. M., Crotwell, A. M., Miller, J. B., and Gatti, L. V.: Observational constraints on recent increases in the atmospheric CH<sub>4</sub> burden, *Geophysical Research Letters*, 36, <http://dx.doi.org/10.1029/2009GL039780>, 118803, 2009.
- Drummond, R., Vandaele, A.-C., Daerden, F., Fussen, D., Mahieux, A., Neary, L., Neefs, E., Robert, S., Willame, Y., and Wilquet, V.: Studying methane and other trace species in the Mars atmosphere using a SOIR instrument, *Planetary and Space Science*, 59, 292–298, <http://www.sciencedirect.com/science/article/pii/S0032063310001479>, 2011.
- Frankenberg, C., Meirink, J. F., Bergamaschi, P., Goede, A. P. H., Heimann, M., Körner, S., Platt, U., van Weele, M., and Wagner, T.: Satellite cartography of atmospheric methane from SCIAMACHY on board ENVISAT: Analysis of the years 2003 and 2004, *Journal of Geophysical Research: Atmospheres*, 111, <http://dx.doi.org/10.1029/2005JD006235>, d07303, 2006.
- 10 García, O. E., Sepúlveda, E., Schneider, M., Wiegeler, A., Borger, C., Hase, F., Barthlott, S., Blumenstock, T., and de Frutos, A. M.: Upper tropospheric CH<sub>4</sub> and N<sub>2</sub>O retrievals from MetOp/IASI within the project MUSICA, *Atmospheric Measurement Techniques Discussions*, 2017, 1–32, <https://www.atmos-meas-tech-discuss.net/amt-2016-326/>, 2017.
- Hu, H., Hasekamp, O., Butz, A., Galli, A., Landgraf, J., Aan de Brugh, J., Borsdorff, T., Scheepmaker, R., and Aben, I.: The operational methane retrieval algorithm for TROPOMI, *Atmospheric Measurement Techniques*, 9, 5423–5440, <https://www.atmos-meas-tech.net/9/5423/2016/>, 2016.
- 15 Huijnen, V., Williams, J., van Weele, M., van Noije, T., Krol, M., Dentener, F., Segers, A., Houweling, S., Peters, W., de Laat, J., Boersma, F., Bergamaschi, P., van Velthoven, P., Le Sager, P., Eskes, H., Alkemade, F., Scheele, R., Nédélec, P., and Pätz, H.-W.: The global chemistry transport model TM5: description and evaluation of the tropospheric chemistry version 3.0, *Geoscientific Model Development*, 3, 445–473, <https://www.geosci-model-dev.net/3/445/2010/>, 2010.
- 20 Hultberg, T.: IASI Principal Component Compression (IASI PCC) FAQ and IASI Level 1 PCC Product Format Specification, Technical notes, <http://www.eumetsat.int/website/home/Data/Products/Level1Data/index.html?lang=EN>, 2009.
- Jacob, D. J., Turner, A. J., Maasackers, J. D., Sheng, J., Sun, K., Liu, X., Chance, K., Aben, I., McKeever, J., and Frankenberg, C.: Satellite observations of atmospheric methane and their value for quantifying methane emissions, *Atmospheric Chemistry and Physics*, 16, 14371–14396, <https://www.atmos-chem-phys.net/16/14371/2016/>, 2016.
- 25 Jardine, C., Boardman, B., Osman, A., Vowles, J., and Palmer, J. e.: Methane UK, <http://www.eci.ox.ac.uk/research/energy/archive-methane.html>, 2009.
- Karion, A., Sweeney, C., Tans, P., and Newberger, T.: AirCore: An Innovative Atmospheric Sampling System, *Journal of Atmospheric and Oceanic Technology*, 27, 1839–1853, <https://doi.org/10.1175/2010JTECHA1448.1>, 2010.
- Kirschke, S., Bousquet, P., Ciais, P., Saunoy, M., Canadell, J., Dlugokencky, E., Bergamaschi, P., Bergmann, D., Blake, D., Bruhwiler, L., Cameron-Smith, P., Castaldi, S., Chevallier, F., Feng, L., Fraser, A., Heimann, M., Hodson, E., Houweling, S., Josse, B., Fraser, P., Krummel, P., Lamarque, J.-F., Langenfelds, R., Le Quere, C., Naik, V., O’Doherty, S., Palmer, P., Pison, I., Plummer, D., Poulter, B., Prinn, R., Rigby, M., Ringeval, B., Santini, M., Schmidt, M., Shindell, D., Simpson, I., Spahni, R., Steele, L., Strode, S., Sudo, K., Szopa, S., Van Der Werf, G., Voulgarakis, A., Van Weele, M., Weiss, R., Williams, J., and Zeng, G.: Three decades of global methane sources and sinks, *Nature Geoscience*, 6, 813–823, doi:10.1038/ngeo1955, 2013.
- 30 Krol, M., Houweling, S., Bregman, B., van den Broek, M., Segers, A., van Velthoven, P., Peters, W., Dentener, F., and Bergamaschi, P.: The two-way nested global chemistry-transport zoom model TM5: algorithm and applications, *Atmospheric Chemistry and Physics*, 5, 417–432, <https://www.atmos-chem-phys.net/5/417/2005/>, 2005.

- Kuze, A., Suto, H., Shiomi, K., Kawakami, S., Tanaka, M., Ueda, Y., Deguchi, A., Yoshida, J., Yamamoto, Y., Kataoka, F., Taylor, T. E., and Buijs, H. L.: Update on GOSAT TANSO-FTS performance, operations, and data products after more than 6 years in space, *Atmospheric Measurement Techniques*, 9, 2445–2461, <https://www.atmos-meas-tech.net/9/2445/2016/>, 2016.
- Membrive, O., Crevoisier, C., Sweeney, C., Danis, F., Hertzog, A., Engel, A., Bönisch, H., and Picon, L.: AirCore-HR: a high-resolution column sampling to enhance the vertical description of CH<sub>4</sub> and CO<sub>2</sub>, *Atmospheric Measurement Techniques*, 10, 2163–2181, <https://www.atmos-meas-tech.net/10/2163/2017/>, 2017.
- Mishchenko, M. and Travis, L.: Capabilities and limitations of a current Fortran implementation of the T-matrix method for randomly oriented, rotationally symmetric scatterers., *Journal of Quantitative Spectroscopy and Radiative Transfer*, 3, 309–324, 1998.
- Myhre, G., Shindell, D., Breon, F.-M., Collins, W., Fuglestedt, J., Huang, J., Koch, D., Lamarque, J.-F., Lee, D., Mendoza, B., Nakajima, T., Robock, A., Stephens, G., Takemura, T., and Zhang, H.: Anthropogenic and Natural Radiative Forcing, book section 8, p. 659–740, Cambridge University Press, Cambridge, United Kingdom and New York, NY, USA, doi:10.1017/CBO9781107415324.018, [www.climatechange2013.org](http://www.climatechange2013.org), 2013.
- Nisbet, E. G., Dlugokencky, E. J., and Bousquet, P.: Methane on the Rise—Again, *Science*, 343, 493–495, <http://science.sciencemag.org/content/343/6170/493>, 2014.
- Pierangelo, C., Millet, B., Esteve, F., Alpers, M., Ehret, G., Flamant, P., Berthier, S., Gibert, F., Chomette, O., Edouart, D., Deniel, C., Bousquet, P., and Chevallier, F.: MERLIN (Methane Remote Sensing Lidar Mission): An Overview, vol. 119, p. 26001, EPJ (European Physical Journal) Web of Conferences, doi:10.1051/epconf/201611926001, 2016.
- Razavi, A., Clerbaux, C., Wespes, C., Clarisse, L., Hurtmans, D., Payan, S., Camy-Peyret, C., and Coheur, P. F.: Characterization of methane retrievals from the IASI space-borne sounder, *Atmospheric Chemistry and Physics*, 9, 7889–7899, <https://www.atmos-chem-phys.net/9/7889/2009/>, 2009.
- Robert, S., Vandaele, A., Thomas, I., Willame, Y., Daerden, F., Delanoye, S., Depiesse, C., Drummond, R., Neefs, E., Neary, L., Ristic, B., Mason, J., Lopez-Moreno, J.-J., Rodriguez-Gomez, J., Patel, M., and Bellucci, G.: Expected performances of the NOMAD/ExoMars instrument, *Planetary and Space Science*, 124, 94–104, <http://www.sciencedirect.com/science/article/pii/S0032063315301203>, 2016.
- Rodgers, C. D.: *Inverse methods for atmospheric sounding: Theory and practice*, World Scientific, 2000.
- Rodgers, C. D. and Connor, B. J.: Intercomparison of remote sounding instruments, *Journal of Geophysical Research: Atmospheres*, 108, <http://dx.doi.org/10.1029/2002JD002299>, 4116, 2003.
- Rothman, L., Gordon, I., Babikov, Y., Barbe, A., Benner, D. C., Bernath, P., Birk, M., Bizzocchi, L., Boudon, V., Brown, L., Campargue, A., Chance, K., Cohen, E., Coudert, L., Devi, V., Drouin, B., Fayt, A., Flaud, J.-M., Gamache, R., Harrison, J., Hartmann, J.-M., Hill, C., Hodges, J., Jacquemart, D., Jolly, A., Lamouroux, J., Roy, R. L., Li, G., Long, D., Lyulin, O., Mackie, C., Massie, S., Mikhailenko, S., Müller, H., Naumenko, O., Nikitin, A., Orphal, J., Perevalov, V., Perrin, A., Polovtseva, E., Richard, C., Smith, M., Starikova, E., Sung, K., Tashkun, S., Tennyson, J., Toon, G., Tyuterev, V., and Wagner, G.: The HITRAN2012 molecular spectroscopic database, *Journal of Quantitative Spectroscopy and Radiative Transfer*, 130, 4 – 50, <http://www.sciencedirect.com/science/article/pii/S0022407313002859>, HITRAN2012 special issue, 2013.
- Saunois, M., Jackson, R. B., Bousquet, P., Poulter, B., and Canadell, J. G.: The growing role of methane in anthropogenic climate change, *Environmental Research Letters*, 11, 120207, <http://stacks.iop.org/1748-9326/11/i=12/a=120207>, 2016.
- Shindell, D., Kuylenstierna, J. C. I., Vignati, E., van Dingenen, R., Amann, M., Klimont, Z., Anenberg, S. C., Muller, N., Janssens-Maenhout, G., Raes, F., Schwartz, J., Faluvegi, G., Pozzoli, L., Kupiainen, K., Höglund-Isaksson, L., Emberson, L., Streets, D., Ramanathan, V.,

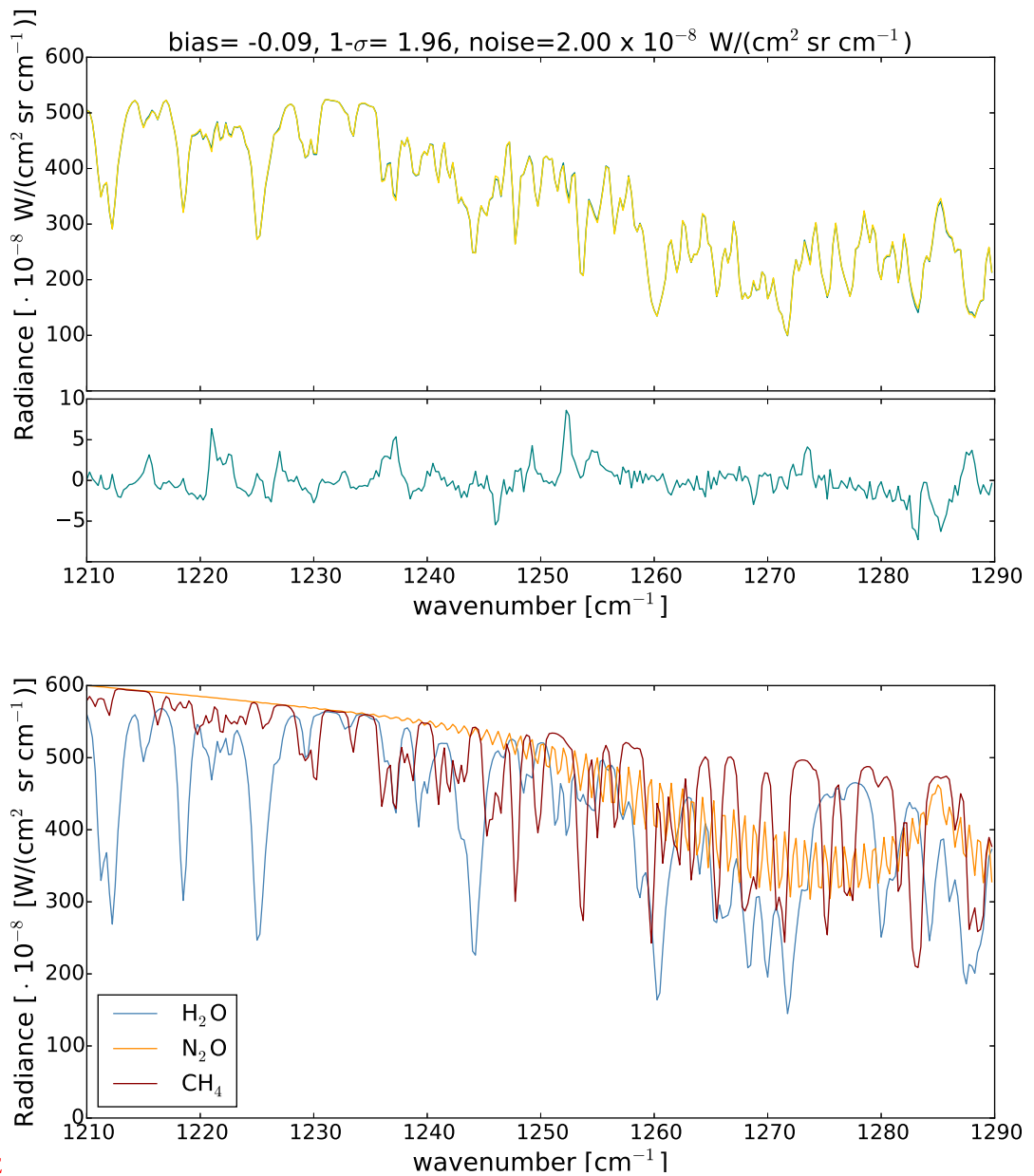
- Hicks, K., Oanh, N. T. K., Milly, G., Williams, M., Demkine, V., and Fowler, D.: Simultaneously Mitigating Near-Term Climate Change and Improving Human Health and Food Security, *Science*, 335, 183–189, <http://science.sciencemag.org/content/335/6065/183>, 2012.
- Siddans, R., Knappett, D., Waterfall, A., Hurley, J., Latter, B., Kerridge, B., Boesch, H., and Parker, R.: Global height-resolved methane retrievals from the Infrared Atmospheric Sounding Interferometer (IASI) on MetOp, *Atmospheric Measurement Techniques Discussions*, 5, 2016, 1–46, <https://www.atmos-meas-tech-discuss.net/amt-2016-290/>, 2016.
- Spurr, R. J.: VLIDORT: A linearized pseudo-spherical vector discrete ordinate radiative transfer code for forward model and retrieval studies in multilayer multiple scattering media, *Journal of Quantitative Spectroscopy and Radiative Transfer*, 102, 316–342, <http://www.sciencedirect.com/science/article/pii/S0022407306001191>, 2006.
- van Weele, M., Williams, J. E., van Velthoven, P. F., Schuck, T. J., and Brenninkmeijer, C. A.: Methane variability in the upper troposphere and lower stratosphere and their relevance for emission inversions constrained by satellite observations, vol. 6, *Conference Proceedings Non CO2 Greenhouse Gases*, 2011.
- Vandaele, A., Kruglanski, M., and De Mazière, M.: Modelling and retrieval of Atmospheric spectra using ASIMUT, *Proc. of the First Atmospheric Science Conference*, 2006.
- Vandaele, A. C., De Mazière, M., Drummond, R., Mahieux, A., Neefs, E., Wilquet, V., Korabiev, O., Fedorova, A., Belyaev, D., Montmessin, F., and Bertaux, J.-L.: Composition of the Venus mesosphere measured by Solar Occultation at Infrared on board Venus Express, *Journal of Geophysical Research: Planets*, 113, <http://dx.doi.org/10.1029/2008JE003140>, e00B23, 2008.
- Vandenbussche, S., Kochenova, S., Vandaele, A. C., Kumps, N., and De Mazière, M.: Retrieval of desert dust aerosol vertical profiles from IASI measurements in the TIR atmospheric window, *Atmospheric Measurement Techniques*, 6, 2577–2591, <https://www.atmos-meas-tech.net/6/2577/2013/>, 2013.
- 20 Vigouroux, C., Hendrick, F., Stavrou, T., Dils, B., De Smedt, I., Hermans, C., Merlaud, A., Scolas, F., Senten, C., Vanhaelewyn, G., Fally, S., Carleer, M., Metzger, J.-M., Müller, J.-F., Van Roozendael, M., and De Mazière, M.: Ground-based FTIR and MAX-DOAS observations of formaldehyde at Réunion Island and comparisons with satellite and model data, *Atmospheric Chemistry and Physics*, 9, 9523–9544, <https://www.atmos-chem-phys.net/9/9523/2009/>, 2009.
- WMO: WMO 2016 News Bulletin, <http://www.wmo.int/pages/prog/arep/gaw/ghg/GHGbulletin.html>, 2016.
- 25 Worden, J., Kulawik, S., Frankenberg, C., Payne, V., Bowman, K., Cady-Peirara, K., Wecht, K., Lee, J.-E., and Noone, D.: Profiles of CH<sub>4</sub>, HDO, H<sub>2</sub>O, and N<sub>2</sub>O with improved lower tropospheric vertical resolution from Aura TES radiances, *Atmospheric Measurement Techniques*, 5, 397–411, <https://www.atmos-meas-tech.net/5/397/2012/>, 2012.
- Xiong, X., Barnet, C., Maddy, E., Sweeney, C., Liu, X., Zhou, L., and Goldberg, M.: Characterization and validation of methane products from the Atmospheric Infrared Sounder (AIRS), *Journal of Geophysical Research: Biogeosciences*, 113, <http://dx.doi.org/10.1029/2007JG000500>, g00A01, 2008.
- 30 Xiong, X., Barnet, C. D., Zhuang, Q., Machida, T., Sweeney, C., and Patra, P. K.: Mid-upper tropospheric methane in the high Northern Hemisphere: Spaceborne observations by AIRS, aircraft measurements, and model simulations, *Journal of Geophysical Research: Atmospheres*, 115, <http://dx.doi.org/10.1029/2009JD013796>, d19309, 2010.
- Xiong, X., Barnet, C., Maddy, E. S., Gambacorta, A., King, T. S., and Wofsy, S. C.: Mid-upper tropospheric methane retrieval from IASI and its validation, *Atmospheric Measurement Techniques*, 6, 2255–2265, <https://www.atmos-meas-tech.net/6/2255/2013/>, 2013.
- 35 Zhou, D. K., Larar, A. M., Liu, X., Smith, W. L., Strow, L. L., Yang, P., Schlüssel, P., and Calbet, X.: Global Land Surface Emissivity Retrieved From Satellite Ultraspectral IR Measurements, *IEEE Trans. Geoscience and Remote Sensing*, 49, 1277–1290, 2011.

- Calisesi, Y., V.T. Soebijanta, and R. van Oss (2005), Regridding of remote soundings: Formulation and application to ozone profile comparison, *J. Geophys. Res.*, 110, D23306, doi:10.1029/2005JD006122.
- 5 Clerbaux, C., Boynard, A., Clarisse, L., George, M., Hadji-Lazaro, J., Herbin, H., Hurtmans, D., Pommier, M., Razavi, A., Turquety, S., Wespes, C. and Coheur, P.-F.: Monitoring of atmospheric composition using the thermal infrared IASI/MetOp  
5 sounder, *Atmos. Chem. Phys.*, 9, 6041-6054, 2009.
- Clerbaux, C., Coheur, P.-F., Bauduin, S., Boynard, A., Clarisse, L., et al., Doniki, S., George, M., Hadji-Lazaro, J., Hurtmans, D., Lacour, J.-L., Ronsmans, G., Van Damme, M., Wespes, C. and Whitburn, S., Tracking pollutants from space: 10 years of IASI satellite observation, *IGAC 2016 Science Conference (International Global Atmospheric Chemistry)*, Sep. 2016, Breckenridge, United States.
- 10 Crevoisier, C., Nobileau, D., Fiore, A. M., Armante, R., Chédin, A., and Scott, N. A.: Tropospheric methane in the tropics –first year from IASI hyperspectral infrared observations, *Atmos. Chem. Phys.*, 9, 6337-6350, doi:10.5194/acp-9-6337-2009, 2009.
- De Wachter, E., Barret, B., Le Flochmoën, E., Pavelin, E., Matricardi, M., Clerbaux, C., Hadji-Lazaro, J., George, M., Hurtmans, D., Coheur, P.-F., Nedelec, P., and Cammas, J.-P.: Retrieval of MetOp-A/IASI CO profiles and validation with  
15 MOZAIC data, *Atmos. Meas. Tech.*, 5, 2843-2857, doi:10.5194/amt-5-2843-2012, 2012.
- Dlugokencky, E.J., Houweling, S., Bruhwiler, L., Masarie, K.A., Lang, P.M., Miller, J.B. and Tans, P.P. 2003. Geophysical Research Letters 30: 10.1029/2003GL018126.
- Dlugokencky, E. J.; Bruhwiler, L.; White, J. W. C.; Emmons, L. K.; Novelli, P. C.; Montzka, S. A.; Masarie, K. A.; Lang, P. M.; Crotwell, A. M.; Miller, J. B. and Gatti, L. V., Observational constraints on recent increases in the atmospheric CH4  
20 burden, *Geophys. Res. Lett.*, 36, L18803, doi:10.1029/2009GL039780.
- Vandaele, A.-C., Daerden, F., Fussen, D., Mahieux, A., Neary, L., Neefs, E., Robert, S., Willame, Y., Wilquet, V., Studying methane and other trace species in the Mars atmosphere using a SOIR instrument Original Research Article, *Planet. Space Sci.* 59, 292-298.
- Frankenberg, C., Meirink, J. F., Bergamaschi, P., Goede, A. P. H., Heimann, M., Körner, S., Platt, U., van Weele, M., and  
25 Wagner, T.: Satellite cartography of atmospheric methane from SCIAMACHY on board ENVISAT: Analysis of the years 2003 and 2004, *J. Geophys. Res.*, 111, D07303, doi:10.1029/2005JD006235, 2006.
- García, O. E., Sepveda, E., Schneider, M., Wiegeler, A., Borger, C., Hase, F., Barthlott, S., Blumenstock, T., and de Frutos, M.: Upper tropospheric CH4 and N2O retrievals from MetOp/IASI within the project MUSICA, *Atmos. Meas. Tech. Discuss.*, doi:10.5194/amt-2016-326, in review, 2017.
- 30 Hu, H., Hasekamp, O., Butz, A., Galli, A., Landgraf, J., Aan de Brugh, J., Borsdorff, T., Scheepmaker, R., and Aben, I., The operational methane retrieval algorithm for TROPOMI, *Atmos. Meas. Tech.*, 9, 5423-5440, doi:10.5194/amt-9-5423-2016, 2016.
- Huijnen, V., Williams, J., van Weele, M., van Noije, T., Krol, M., Dentener, F., Segers, A., Houweling, S., Peters, W., de Laat, J., Boersma, F., Bergamaschi, P., van Velthoven, P., Le Sager, P., Eskes, H., Alkemade, F., Scheele, R., Nédélec, P., and

- Pätz, H.-W.: The global chemistry transport model TM5: description and evaluation of the tropospheric chemistry version 3.0, *Geosci. Model Dev.*, 3, 445–473, doi:10.5194/gmd-3-445-2010, 2010.
- Hultberg, T.: IASI Principal Component Compression (IASI PCC) FAQ and IASI Level 1 PCC Product Format Specification, Technical notes, available online at: , 2009.
- 5 Jacob, D. J., Turner, A. J., Maasakkers, J. D., Sheng, J., Sun, K., Liu, X., Chance, K., Aben, I., McKeever, J., and Frankenberg, C.: Satellite observations of atmospheric methane and their value for quantifying methane emissions, *Atmos. Chem. Phys.*, 16, 14371–14396, doi:10.5194/acp-16-14371-2016, 2016.
- Jardine, C.N., Boardman, B., Osman, A., Vowles, J. and Palmer, J. (eds) Methane UK. Environmental Change Institute, University of Oxford, 64–71.
- 10 Karion, A., Sweeney, C., Tans, P., and Newberger, T.: AirCore: An Innovative Atmospheric Sampling System, *Journal of Atmospheric and Oceanic Technology*, 27, 1839–1853, doi:10.1175/2010JTECHA1448.1, , 2010.
- Kirschke, S., Bousquet, P., Ciais, P., Saunois, M., Canadell, J. G., Dlugokencky, E. J., Bergamaschi, P., Bergmann, D., Blake, D. R., Bruhwiler, L., Cameron-Smith, P., Castaldi, S., Chevallier, F., Feng, L., Fraser, A., Heimann, M., Hodson, E. L., Houweling, S., Josse, B., Fraser, P. J., Krummel, P. B., Lamarque, J.-F., Langenfelds, R. L., Le Quere, C., Naik, V., O'Doherty, S., Palmer, P. I., Pison, I., Plummer, D., Poulter, B., Prinn, R. G., Rigby, M., Ringeval, B., Santini, M., Schmidt, M., Shindell, D. T., Simpson, I. J., Spahni, R., Steele, L. P., Strode, S. A., Sudo, K., Szopa, S., Van Der Werf, G. R., Voulgarakis, A., Van Weele, M., Weiss, R. F., Williams, J. E. and Zeng, G. Three decades of global methane sources and sinks *Nature Geoscience*, Nature Publishing Group, 2013, 6, 813–823.
- 15 Krol, M., Houweling, S., Bregman, B., van den Broek, M., Segers, A., van Velthoven, P., Peters, W., Dentener, F., and Bergamaschi, P.: The two-way-nested global-chemistry-transport zoom model TM5: algorithm and applications, *Atmos. Chem. Phys.*, 5, 417–432, doi:10.5194/acp-5-417-2005, 2005.
- 20 Kuze, A., Suto, H., Shiomi, K., Kawakami, S., Tanaka, M., Ueda, Y., Deguchi, A., Yoshida, J., Yamamoto, Y., Kataoka, F., Taylor, T. E., and Buijs, H. L.: Update on GOSAT TANSO-FTS performance, operations, and data products after more than 6 years in space, *Atmos. Meas. Tech.*, 9, 2445–2461, doi:10.5194/amt-9-2445-2016, 2016.
- 25 Membrive, O., Crevoisier, C., Sweeney, C., Danis, F., Hertzog, A., Engel, A., Bönisch, H., and Picon, L.: AirCore-HR: A high-resolution column sampling to enhance the vertical description of CH<sub>4</sub> and CO<sub>2</sub>, *Atmos. Meas. Tech. Discuss.*, doi:10.5194/amt-2016-236, in review, 2016.
- Mishechenko, M.I., Travis, L.D., 1998. Capabilities and limitations of a current Fortran implementation of the T-matrix method for randomly oriented, rotationally symmetric scatterers. *J. Quant. Spectrosc. Radiat. Transf.* 60 (3), 309–324.
- 30 Myhre, G., D. Shindell, F. M. Bréon, W. Collins, J. Fuglestad, J. Huang, D. Koch, J.-F. Lamarque, D. Lee, B. Mendoza, T. Nakajima, A. Robock, G. Stephens, T. Takemura and H. Zhang, 2013: Anthropogenic and Natural Radiative Forcing. In: *Climate Change 2013: The Physical Science Basis. Contribution of Working Group I to the Fifth Assessment Report of the Intergovernmental Panel on Climate Change* Stocker, T.F., D. Qin, G. K. Plattner, M. Tignor, S.K. Allen, J. Boschung, A. Nauels, Y. Xia, V. Bex and P.M. Midgley (eds.). Cambridge University Press, Cambridge, United Kingdom and New York, NY, USA.
- 35

- Nisbet, E. G., E. J. Dlugokencky, and P. Bousquet (2014), Methane on the rise—Again, *Science*, 343, 493–5.
- Patra, P. K., X. Xiong, C. Barnett, E. J. Dlugokencky, U. Karin, K. Tsuboi, and D. Worthy, Validation of CH<sub>4</sub> surface emission using forward chemistry-transport model, Baltimore, April 2009.
- C. Pierangelo, B. Millet, F. Esteve, M. Alpers, G. Ehret, P. Flamant, S. Berthier, F. Gibert, O. Chomette, D. Edouart,  
5 C. Deniel, P. Bousquet and F. Chevallier, MERLIN (Methane Remote Sensing Lidar Mission): an Overview, EPJ Web of Conferences 119-26001 (2016), DOI: 10.1051/epjconf/201611926001
- Razavi, A., Clerbaux, C., Wespes, C., Clarisse, L., Hurtmans, D., Payan, S., Camy-Peyret, C., and Coheur, P. F.: Characterization of methane retrievals from the IASI space-borne sounder, *Atmos. Chem. Phys.*, 9, 7889–7899, doi:10.5194/acp-9-7889-2009, 2009.
- 10 Robert, S., Vandaele, A.C., Thomas, I., Willame, Y., Daerden, F., Delanoye, S., Depiesse, C., Drummond, R., Neefs, E., Neary, L., Ristic, B., Mason, J., Lopez-Moreno, J.-J., Rodriguez-Gomez, J., Patel, M.R., Bellucci, G., The NOMAD Team., Expected performances of the NOMAD/ExoMars instrument. *Planetary and Space Science* (2016), <http://dx.doi.org/10.1016/j.pss.2016.03>.
- Rodgers, C.D.: *Inverse methods for atmospheric sounding: Theory and Practice*. Singapore: World Scientific Publishing Co. Pte. Ltd., 2000.
- 15 Rodgers, C.D. and Connor, B.J.: Intercomparison of remote sounding instruments, *J. Geophys. Res.*, 108, 4116–4129, 2003.
- Rothman, L., Gordon, I., Babikov, Y., Barbe, A., Benner, D. C., Bernath, P., Birk, M., Bizzocchi, L., Boudon, V., Brown, L., Campargue, A., Chance, K., Cohen, E., Coudert, L., Devi, V., Drouin, B., Fayt, A., Flaud, J.-M., Gamache, R., Harrison, J., Hartmann, J.-M., Hill, C., Hodges, J., Jacquemart, D., Jolly, A., Lamouroux, J., Roy, R. L., Li, G., Long, D., Lyulin, O., Mackie, C., Massie, S., Mikhailenko, S., Müller, H., Naumenko, O., Nikitin, A., Orphal, J., Perevalov, V., Perrin, A., Polovtseva, E., Richard, C., Smith, M., Starikova, E., Sung, K., Tashkun, S., Tennyson, J., Toon, G., Tyuterev, V. and Wagner, G., The HITRAN2012 molecular spectroscopic database *Journal of Quantitative Spectroscopy and Radiative Transfer*, 2013, 130, 4–50.
- 20 Siddans, R., Knappett, D., Waterfall, A., Hurley, J., Latter, B., Kerridge, B., Boesch, H., and Parker, R.: Global height-resolved methane retrievals from the Infrared Atmospheric Sounding Interferometer (IASI) on MetOp, *Atmos. Meas. Tech. Discuss.*, doi:10.5194/amt-2016-290, in review, 2016.
- Vandaele, A.C., Kruglanski, M., De Mazière, M., Modelling and retrieval of Atmospheric spectra using ASIMUT in Proc. of the First ‘Atmospheric Science Conference’, ESRIN, Frascati, Italy, 8–12 May 2006.
- 30 Vandaele, A.C., De Mazière, M., Drummond, R., Mahieux, A., Neefs, E., Wilquet, V., Korabely, O., Fedorova, A., Belyaev, D., Montmessin, F., Bertaux, J.-L., 2008. Composition of the Venus mesosphere measured by SOIR on board Venus Express. *J. Geophys. Res.* 113. <http://dx.doi.org/10.1029/2008JE003140>.
- Vandenbussche, S., Kochenova, S., Vandaele, A. C., Kumps, N., De Mazière, M., Retrieval Of Desert Dust Aerosol Vertical Profiles From Iasi Measurements In The Tir Atmospheric Window, *Atmos. Meas. Tech.* 6, 2577–2591, 2013.

- van Weele, M., Williams, J. E., van Velthoven, P. F.J., Schuck, T. J., Brenninkmeijer, C. A.M., Methane variability in the upper troposphere and lower stratosphere and their relevance for emission inversions constrained by satellite observations, Conference Proceedings Non-CO<sub>2</sub> Greenhouse Gases, Amsterdam, Volume: 6, November 2011.
- Worden, J., Kulawik, S., Frankenberg, C., Payne, V., Bowman, K., Cady-Peirara, K., Wecht, K., Lee, J. E., and Noone, D.: Profiles of CH<sub>4</sub>, HDO, H<sub>2</sub>O and N<sub>2</sub>O with improved tropospheric vertical resolution from Aura TES radiances, *Atmos. Meas. Tech.*, 5, 397–411, doi:10.5194/amt-5-397-2012, 2012.
- Saunois, M., Jackson, R. B., Bousquet, P., Poulter, B. and Canadell, J. G. The growing role of methane in anthropogenic climate change *Environmental Research Letters*, 2016, 11, 120207.
- Shindell, D., J.C.I. Kuylenstierna, E. Vignati, R. van Dingenen, M. Amann, Z. Klimont, S.C. Anenberg, N. Müller, G. Janssens-Maenhout, F. Raes, J. Schwartz, G. Faluvegi, L. Pozzoli, K. Kupiainen, L. Höglund-Isaksson, L. Emberson, D. Streets, V. Ramanathan, K. Hicks, N.T.K. Oanh, G. Milly, M. Williams, V. Demkine, and D. Fowler, 2012: Simultaneously mitigating near-term climate change and improving human health and food security. *Science*, 335, 183–189, doi:10.1126/science.1210026.
- Spurr, R.J.D., 2006. VLIDORT: a linearized pseudo-spherical vector discrete ordinate radiative transfer code for forward model and retrieval studies in multilayer multiple scattering media. *J. Quant. Spectrosc. Radiat. Transf.* 102, 316–342.
- Vigouroux, C., Hendrick, F., Stavrakou, T., Dils, B., De Smedt, I., Hermans, C., Merlaud, A., Scolas, F., Senten, C., Vanhaelewyn, G., Fally, S., Carleer, M., Metzger, J. M., Müller, J. F., Van Roozendael, M., and De Mazière, M.: Ground-based FTIR and MAX-DOAS observations of formaldehyde at Réunion Island and comparisons with satellite and model data, *Atmos. Chem. Phys.*, 9, 9523–9544, doi:10.5194/acp-9-9523-2009, 2009.
- Xiong, X., Barnett, C., Maddy, E., Sweeney, C., Liu, X., Zhou, L., and Goldberg, M.: Characterization and validation of methane products from the Atmospheric Infrared Sounder (AIRS), *J. Geophys. Res.*, 113, G00A01, doi:10.1029/2007JG000500, 2008.
- Xiong, X., C. D. Barnett, Q. Zhuang, T. Machida, C. Sweeney, and P. K. Patra (2010), Mid-upper tropospheric methane in the high Northern Hemisphere: Spaceborne observations by AIRS, aircraft measurements, and model simulations, *J. Geophys. Res.*, 115, D19309, doi:10.1029/2009JD013796.
- Xiong, X., Barnett, C., Maddy, E. S., Gambacorta, A., King, T. S., and Wofsy, S. C.: Mid-upper tropospheric methane retrieval from IASI and its validation, *Atmos. Meas. Tech.*, 6, 2255–2265, doi:10.5194/amt-6-2255-2013, 2013.
- Zhou, D.K., Larar, A.M., Liu, X., Smith, W.L., Strow, L.L. and Yang, P.: Global Land Surface Emissivity Retrieved From Satellite Ultraspectral IR Measurements, *IEEE Trans. Geosci. Remote. Sens.*, 49(4), 1277–1290, doi:10.1109/TGRS.2010.2051036, 2011.



MODIFIED FIGURE

**Figure 1.** Top panel : [top] Measured (blue) and simulated (yellow) radiances. [bottom] Measured minus simulated radiances. The mean difference (bias), 1- $\sigma$  standard deviation of the difference and radiometric noise-value used in the retrieval (all in x 10<sup>-8</sup> W/(cm<sup>2</sup> sr cm<sup>-1</sup>)) are given in the title. Bottom panel : Three simulated radiances under the assumption of a single-species atmosphere containing either only CH<sub>4</sub>, H<sub>2</sub>O or N<sub>2</sub>O, showing the contribution of the different prominent molecules in this spectral region.

MODIFIED FIGURE

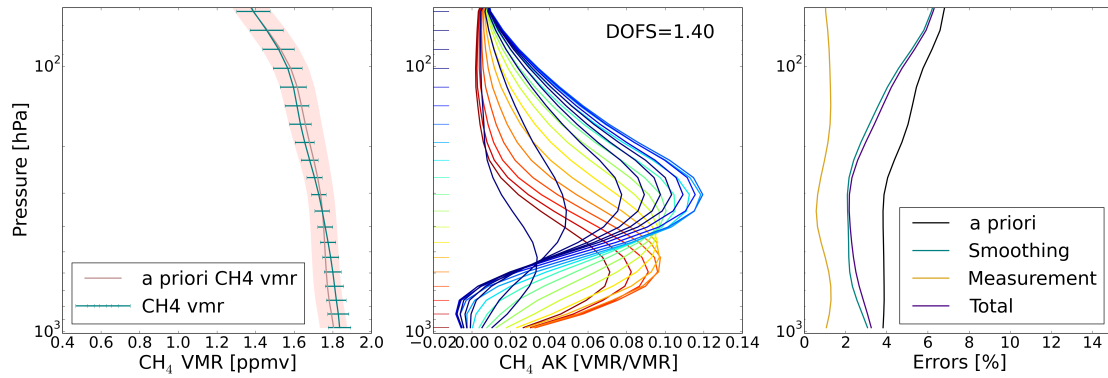


**Figure 2.** [left] Retrieved and a priori CH<sub>4</sub> vmr profile in ppmv for an observation on the 2<sup>nd</sup> of July 2013. The pink shaded area is the a priori variability and the horizontal blue bars are the retrieval uncertainty. [middle] Averaging kernel of the retrieval with a DOFS of 1.40. [right] CH<sub>4</sub> uncertainty profiles in percentage. Given are the measurement (yellow) and smoothing (blue) uncertainty which contribute to the total (purple) uncertainty. The black line represents the variability of the a priori as calculated from the square root of the diagonal elements of the a priori uncertainty covariance matrix  $S_a$ .

CH <sub>4</sub>	
Spectral range	1210-1290 cm <sup>-1</sup>
State vector	CH <sub>4</sub> , H <sub>2</sub> O and N <sub>2</sub> O profile, CO <sub>2</sub> total column, T <sub>skin</sub>
Pressure, temperature, RH	IASI L2
Spectroscopy	HITRAN 2012
Emissivity	Zhou et al. (2011)
a priori information	WACCM + <a href="#">IASI L2</a>

**Table 1.** Characteristics BIRA-IASB CH<sub>4</sub> retrieval.

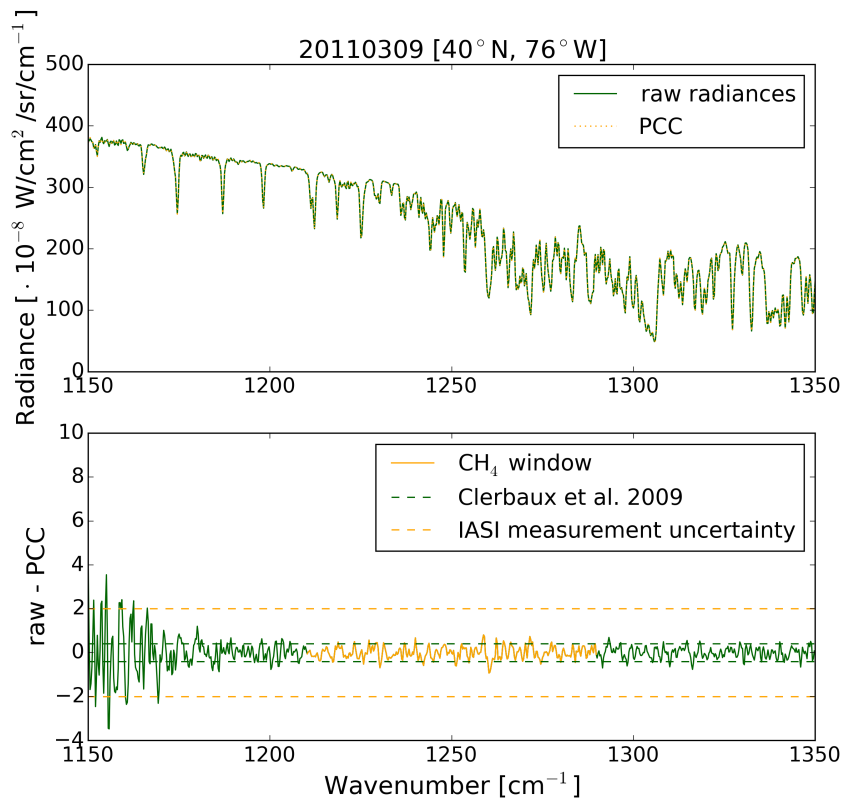


**Figure 3.** Radiances from a nighttime pixel on the 9<sup>th</sup> of March 2011 at 40°N and 76°W. [top] Raw radiances and PCC-reconstructed radiances. [bottom] Difference between raw radiances and PCC radiances. The CH<sub>4</sub> spectral retrieval window is highlighted in orange. The green horizontal dashed lines indicates the IASI radiometric noise at 1250  $\text{cm}^{-1}$  as given by Clerbaux et al. (2009) and the orange horizontal dashed lines indicate the IASI radiometric noise defined in the retrieval (see Sect. 3.1). The differences between the raw and PCC radiances are within the IASI radiometric noise.

MODIFIED FIGURE

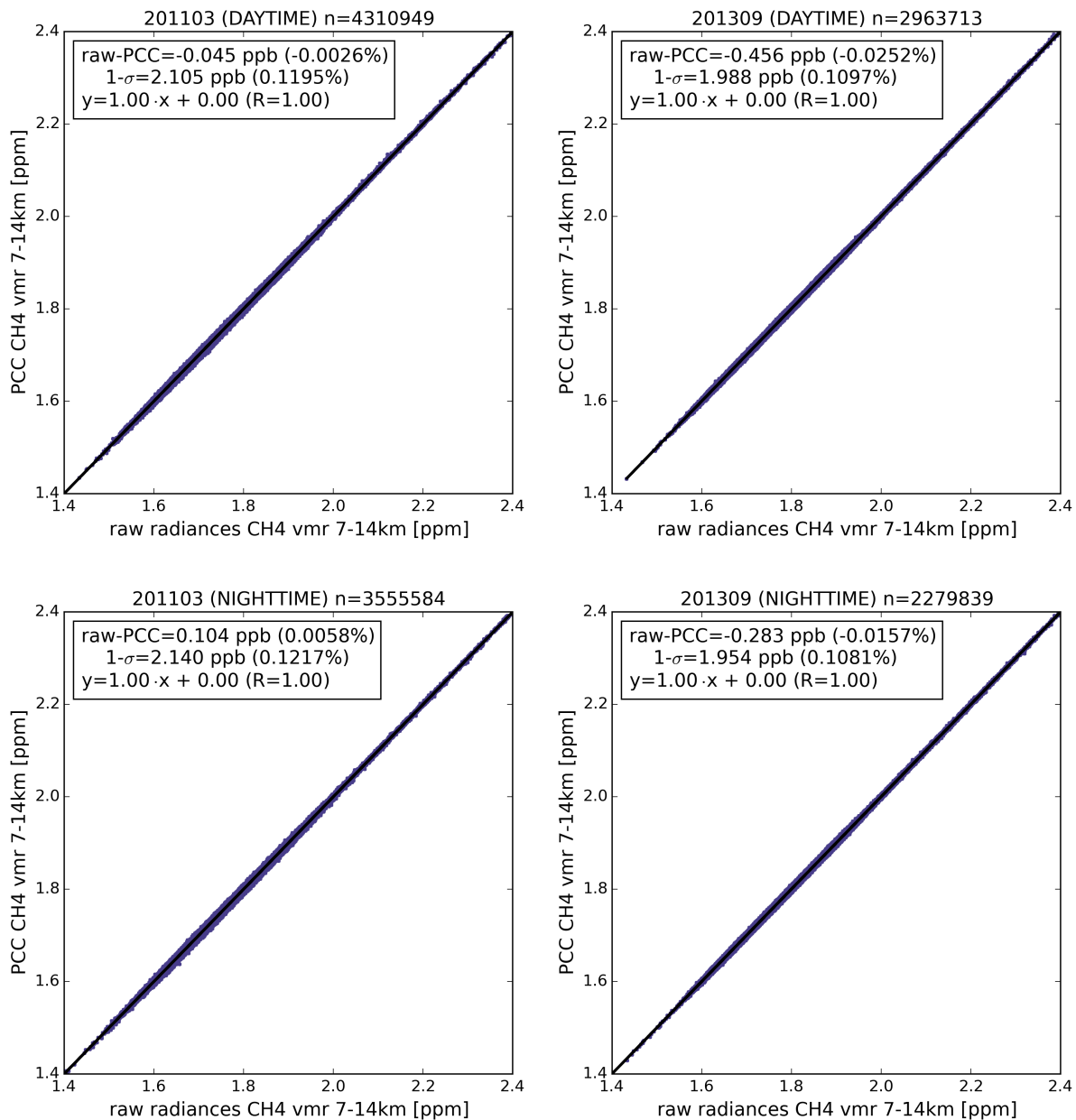
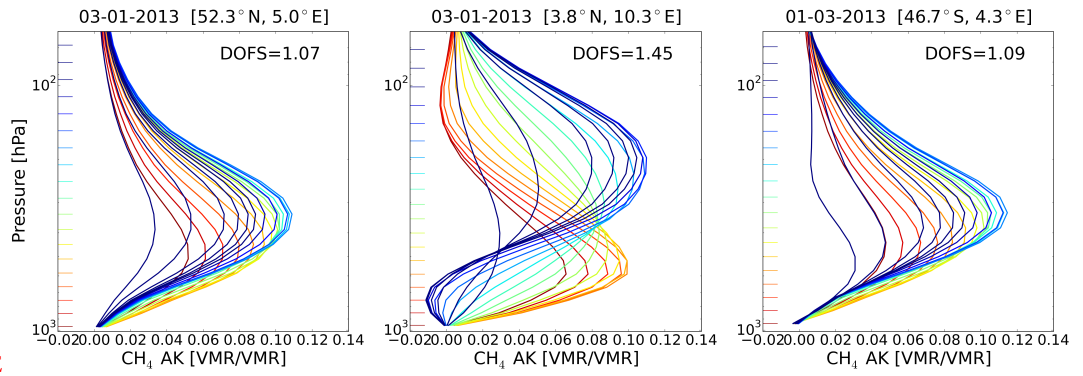


**Figure 4.** Correlation plot retrieved CH<sub>4</sub> between 7 and 14 km from the raw radiances (x-axis) and from the PCC-reconstructed radiances (y-axis) for March 2011 [left] and September 2013 [right], for daytime [top] and nighttime [bottom] retrievals between 60°S and 70°N. The mean difference and 1- $\sigma$  of the difference between raw and PCC partial columns is given in ppb-ppby and % in the legend, as well as the slope and intercept from the least-squares fit and correlation coefficient R.



MODIFIED FIGURE

**Figure 5.** CH<sub>4</sub> averaging kernels for 3 pixels on the 1<sup>st</sup> of March 2013 at 3 different locations (55.2°N, 4°N and 47°S).

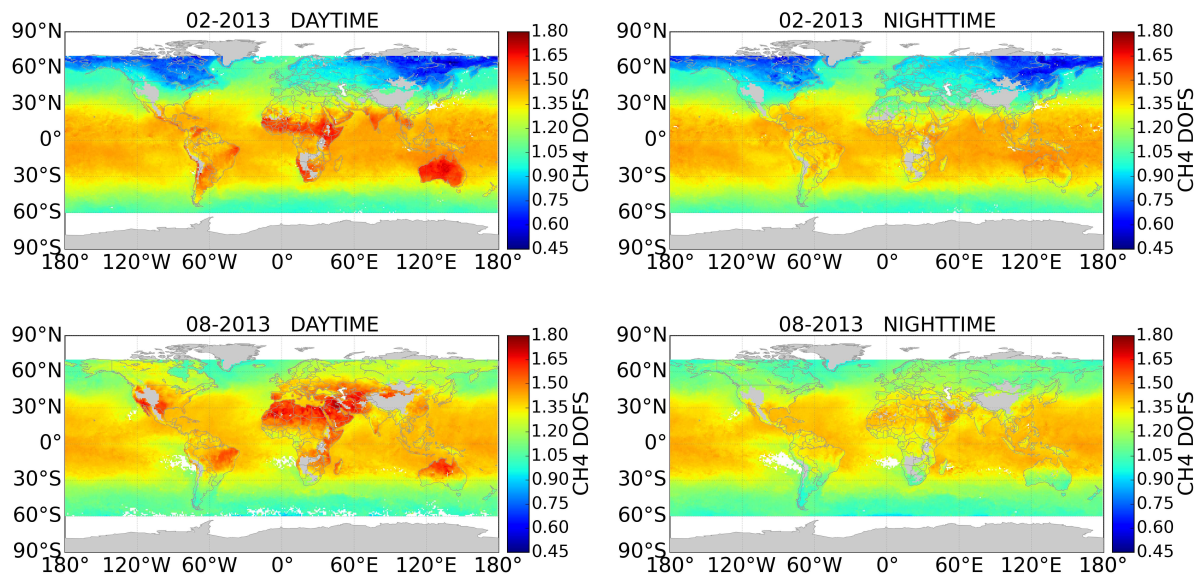


**Figure 6.** Maps of the CH<sub>4</sub> Degrees of Freedom for signal (DOFS) calculated from the trace of the CH<sub>4</sub> averaging kernel, for February [top] and August [bottom] 2013. DOFS for daytime observations are given on the left, DOFS for nighttime observations on the right.

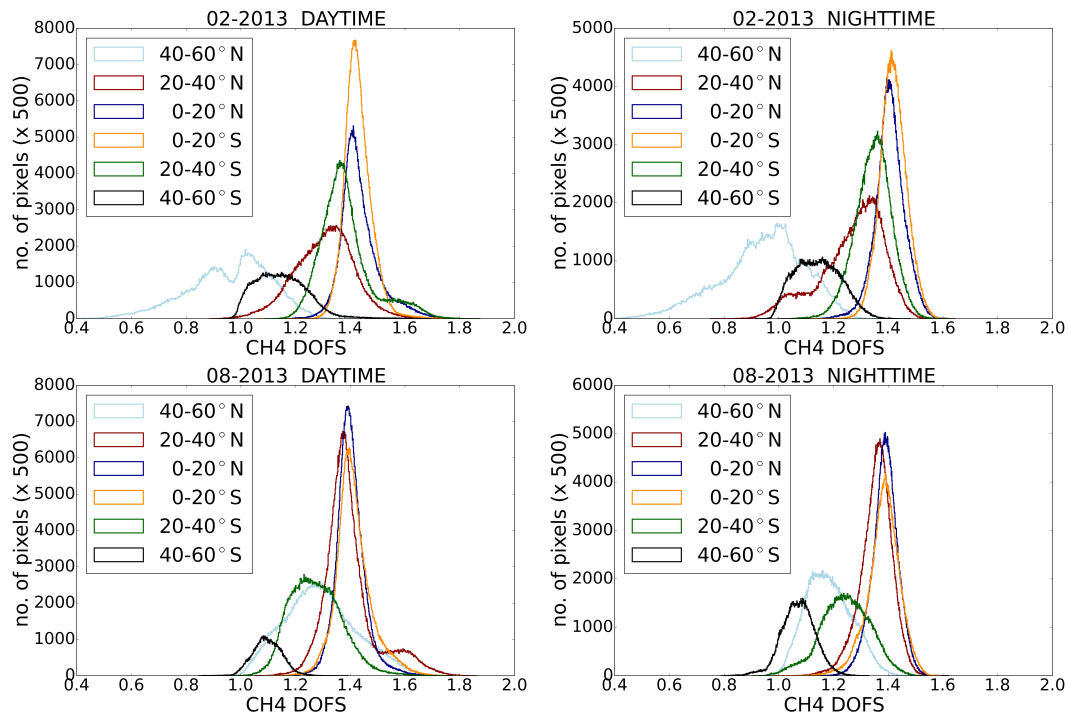


**Figure 7.** CH<sub>4</sub> DOFS for different latitudinal bands for daytime [left] and nighttime [right] observations for February [top] and August [bottom] 2013.

<u>Error Source</u>	<u>Uncertainty Error Source</u>	<u>Uncertainty IASI CH<sub>4</sub></u>
<u>Temperature profile</u>	-	<u>1.40%</u>
<u>CH<sub>4</sub> line intensity</u>	<u>2%</u>	<u>1.93%</u>
<u>CH<sub>4</sub> broadening coefficients</u>	<u>2%</u>	<u>1.09%</u>
<u>CH<sub>4</sub> a priori bias</u>	<u>2%</u>	<u>0.06%</u>
<u>H<sub>2</sub>O line intensity</u>	<u>2%</u>	<u>0.02%</u>
<u>H<sub>2</sub>O broadening coefficients</u>	<u>2%</u>	<u>0.03%</u>
<u>N<sub>2</sub>O line intensity</u>	<u>2%</u>	<u>0.05%</u>
<u>N<sub>2</sub>O broadening coefficients</u>	<u>2%</u>	<u>0.03%</u>
<u>PCC reconstructed</u>	-	<u>0.02%</u>
<u>Emissivity</u>	<u>1%</u>	<u>0.27%</u>
<u>Smoothing</u>	<u>a priori variability</u>	<u>2.45%</u>
<u>Measurement noise</u>	<u><math>2 \cdot 10^{-8} \text{ W}/(\text{cm}^2 \text{ sr cm}^{-1})</math></u>	<u>0.95%</u>
<u>Total</u>		<u>3.73%</u>

**Table 2.** The different error sources (column 1) and their uncertainties considered (column 2) for the IASI CH<sub>4</sub> uncertainty estimation. The results of the uncertainty estimation of the CH<sub>4</sub> 4-17 km partial columns by the perturbation method described in Sect. 4.3 are given in column 3. The uncertainty of the temperature profile on the CH<sub>4</sub> 4-17 km partial column is estimated by replacing the IASI L2 temperature profiles with the ECMWF Era-interim re-analysis temperature profiles. To estimate the uncertainty of the PCC reconstructed spectra on the CH<sub>4</sub> columns we used the raw spectra and compared the retrieved CH<sub>4</sub> partial columns with the PCC reconstructed retrieved CH<sub>4</sub> as is done in Sect. 3.3.

site	LAT	$\Delta$ [%]	$\sigma$ [%]	$\epsilon_{\text{sys}}$ [%]	$\epsilon_{\text{rand}}$ [%]	R	n
Eureka	80°N	<del>-0.51</del> -1.45	<del>3.99</del> -2.05	<del>7.33</del> -7.63	<del>1.98</del> -2.65	<del>0.71</del> 0.67	<del>501</del> -373
Thule	77°N	<del>4.40</del> 4.04	<del>3.65</del> -2.02	<del>5.25</del> -5.28	<del>2.24</del> -2.58	<del>0.84</del> 0.73	<del>244</del> -209
Kiruna	68°N	<del>0.26</del> 0.18	<del>2.20</del> -2.22	<del>3.62</del> -3.59	<del>2.52</del> -2.71	<del>0.88</del> 0.84	<del>445</del> -437
Jungfraujoch	47°N	<del>-0.58</del> -0.95	<del>2.23</del> -2.07	NA	NA	<del>0.96</del> 0.81	<del>737</del> -674
Zugspitze	47°N	<del>-0.13</del> -0.38	<del>2.56</del> -2.48	<del>2.24</del> -2.21	<del>2.33</del> -2.56	<del>0.92</del> 0.68	<del>2123</del> -2020
Toronto	44°N	<del>-1.93</del> -2.31	<del>3.57</del> -2.97	<del>8.32</del> -8.26	<del>3.15</del> -3.21	<del>0.44</del> 0.52	<del>612</del> -535
Izana	28°N	<del>-1.38</del> -1.19	<del>1.91</del> -1.76	<del>3.32</del> -3.29	<del>2.28</del> -2.46	<del>0.90</del> 0.37	<del>3931</del> -3290
Mauna Loa	20°N	<del>0.67</del> -0.17	<del>3.27</del> -1.81	<del>4.81</del> -4.75	<del>2.44</del> -2.48	<del>0.41</del> -0.33	<del>734</del> -592
Maido	21°S	<del>0.25</del> -0.10	<del>3.14</del> -2.54	<del>3.49</del> -3.44	<del>2.90</del> -2.89	<del>0.50</del> 0.15	<del>547</del> -478
Wollongong	34°S	<del>-0.47</del> -0.53	<del>2.24</del> -2.30	6.70	<del>6.20</del> -6.21	<del>0.77</del> 0.60	<del>2293</del> -2230

**Table 3.** Statistics of the comparison between the IASI and smoothed NDACC CH<sub>4</sub> 4-17 km partial columns for the period 2011-2014. For each location, the latitude coordinates, the mean percentage difference ( $\Delta=(\text{IASI}-\text{NDACC})/\text{NDACC}$ ) and standard deviation of the difference ( $\sigma$ ), the mean systematic ( $\epsilon_{\text{sys}}$ ) and random uncertainty of the differences ( $\epsilon_{\text{rand}}$ ), the correlation coefficient (R) and the number of observations (n) are given. NA=not available, for Jungfraujoch the systematic and random uncertainty covariance matrices are not available.

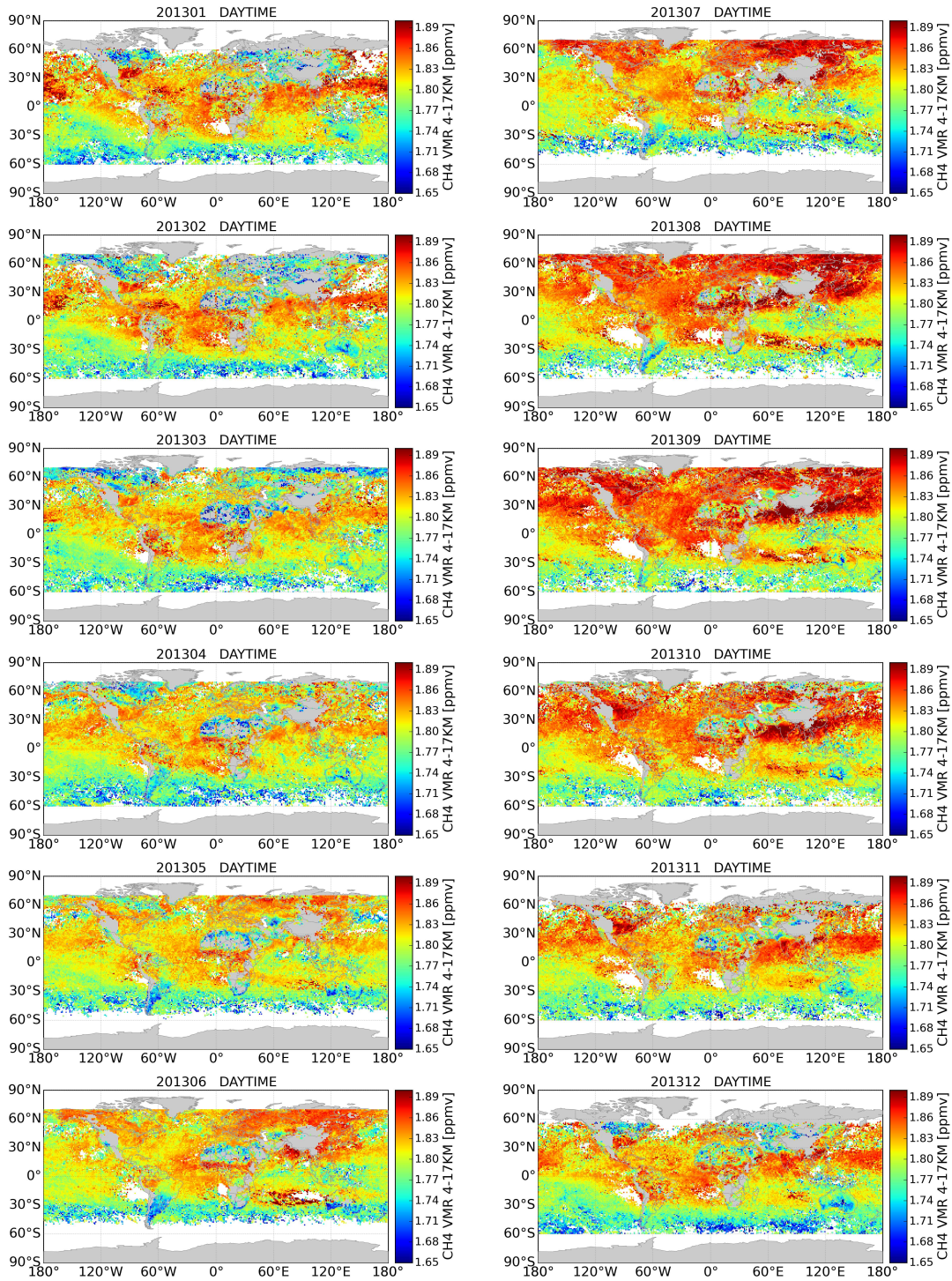


**Figure 8.** Monthly mean global daytime distributions of CH<sub>4</sub> partial columns (4-17 km) in 2013. Given is the average over the 2 x 2 circular pixels which are measured simultaneously by IASI. The pixels are binned on a 1° x 1° grid.

NEW FIGURE

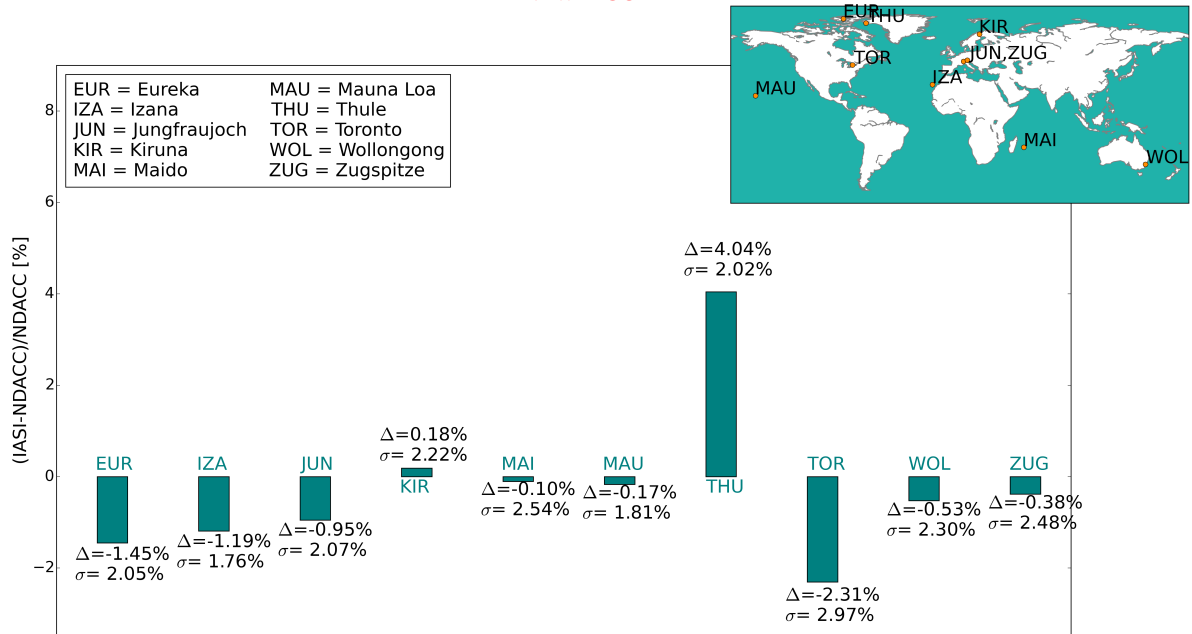


**Figure 9.** Barchart of the results of the IASI-NDACC validation exercise. Given is the relative percentage difference  $\Delta=(IASI-NDACC)/NDACC$  and standard deviation of the difference ( $\sigma$ ) of partial columns in the 4-17 km altitude range for each of the 10 investigated NDACC sites, visualized in the map on the top right. These results are also summarized in Table 3.

NEW FIGURE

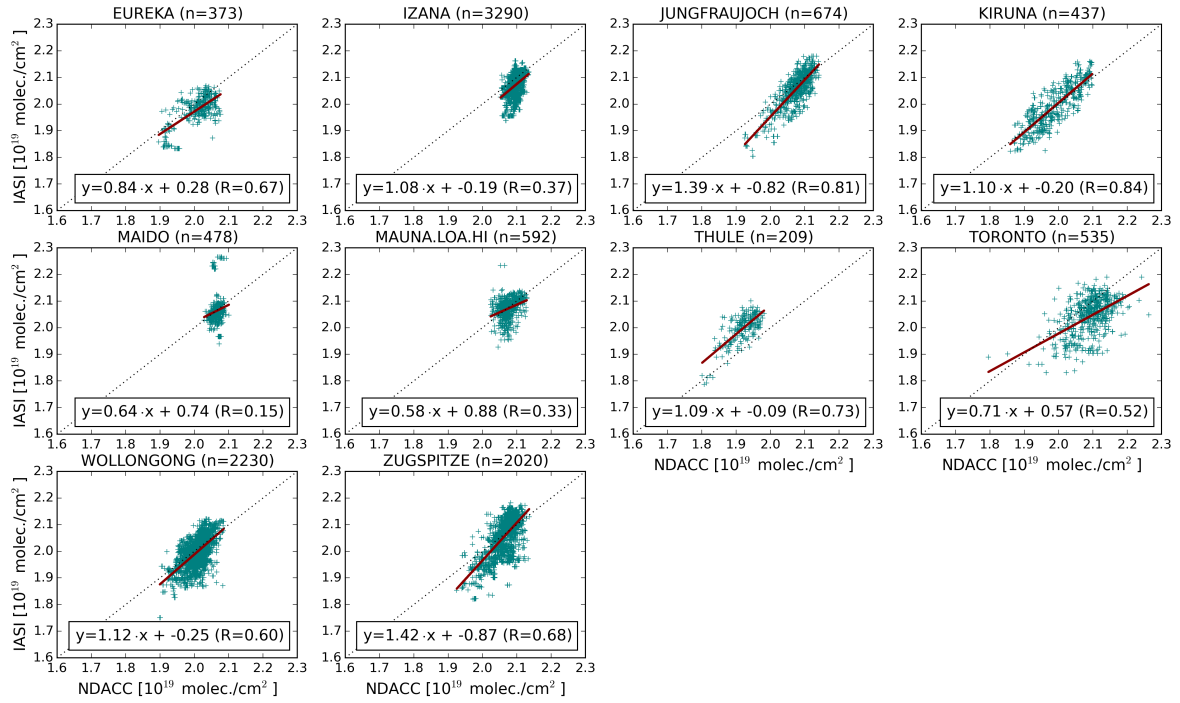


**Figure 10.** Correlation plots of smoothed NDACC and IASI CH<sub>4</sub> partial columns (4-17 km) in molec./cm<sup>2</sup> for the period 2011-2014. The number of collocations (n) is given for each site in the title. The red lines are the linear regressions between the data points and the dashed black line is the unity slope, shown for comparison. The values of the linear regression and the correlation coefficient (R) are given for each station, the latter is summarized in Table 3.